Development of biomaterial porous scaffolds for dendritic cell modulation and mRNA delivery

Ruying Chen

A dissertation

submitted in partial fulfilment of the

requirements for the degree of

Doctor of Philosophy

University of Washington

2017

Reading Committee:

James D. Bryers, Chair

Kim A. Woodrow

Hao Yuan Kueh

Program Authorized to Offer Degree:

Bioengineering

University of Washington

Abstract

Development of biomaterial porous scaffolds for dendritic cell modulation and mRNA delivery

Ruying Chen

Chair of the Supervisory Committee:
Professor James D. Bryers
Department of Bioengineering

mRNA has emerged as a potential candidate for vaccine applications in recent years as a versatile, safe, and cost-effective alternative to traditional therapeutics. Efficient delivery to antigen presenting cells and protection against rapid *in vivo* degradation are the two greatest challenges for mRNA vaccine development. Scaffold based platforms represent a novel and promising approach to improve mRNA vaccine efficacy through cell enrichment, modulation and prolonged local release. This dissertation describes the development of biomaterial porous scaffolds as a platform for dendritic cell modulation and local delivery of mRNA vaccines. First, DCs maturation within scaffolds and the effects of materials and pore sizes were investigated. A series of poly (2-hydroxyethyl methacrylate) (pHEMA) and poly (dimethyl siloxane) (PDMS) were fabricated using the sphere-templating method that generated uniform and interconnected pores with controllable pore size. Scaffolds with smaller pore sizes consistently induced DCs maturation characterized by secretion of pro-inflammatory cytokines and upregulation of surface maturation

markers in both materials *in vitro*. *In vivo* study further revealed that scaffolds with smaller pore sizes favor DC accumulation and maturation at implantation site. At the same time, a minimal throat size among pores is crucial for cell infiltration and potentially gaining access to the therapeutics delivered. Second, a range of polymer and lipid based carriers were evaluated for their ability to facilitate intracellular mRNA delivery and effect on cell viability upon transfection. mRNA lipoplexes formed with Stemfect^{TM} demonstrated excellent capacity in mediating mRNA transfection in a range of cell lines and primary cells with minimal cytotoxicity. Lastly, these lipoplexes with optimized formulation were integrated in HEMA scaffolds through surface adsorption. Scaffold mediated mRNA delivery and expression was demonstrated *in vitro* and *in vivo*. Compared to unformulated mRNA and/or mRNA delivered via subcutaneous bolus injection, formulated mRNA adsorbed on scaffolds lead to prolonged local release, improved mRNA uptake by cells and enhanced transgene expression. Overall, these findings demonstrate the potential of porous biomaterial scaffolds as a platform for dendritic cell modulation and improving the delivery efficiency of mRNA therapeutics.

Table of Contents

List of Figures

List of Tables

List of Abbreviations

APC	antigen presenting cell
BMDC	bone marrow-derived dendritic cell
CLR	C-type lectin receptor
ConA	Concanavalin A
DC	dendritic cell
DLS	dynamic light scattering
DM(A)	dopamine methacrylamide
ELISA	enzyme-linked immunosorbent assay
FBS	fetal bovine serum
GFP	green fluorescence protein
GM-CSF	granulocyte macrophage colony-stimulating factor
iDC	immature dendritic cell
LF-MM	Lipofectamine™ MessengerMAX ™
LN	lymph node
LPEI	*in vivo*-jetPEI®
mRNA	messenger RNA
NTPS	non-treated tissue culture polystyrene
OVA	ovalbumin
PAMP	pathogen-associated molecular pattern
PBAE	poly (β-amino ester)
PDMS	poly (dimethylsiloxane)
pHEMA	poly (2-hydroxyethyl methacrylate)
PMMA	Poly (methyl methacrylate)
PRR	pattern recognition receptor
SEM	scanning electron microscopy
sr-mRNA	self-replicating messenger RNA
ss-mRNA	single stranded messenger RNA
TLR	toll-like receptor

Acknowledgement

I would like to express my sincere gratitude to my advisor Dr. James Bryers for the continuous support of my Ph.D study and related research, for his patience, motivation, and knowledge. I would also like to thank my supervisory committee members, Dr. Buddy Ratner, Dr. Kim Woodrow, Dr. Hao Yuan Kueh, and Dr. Jessica Hammerman, for their support and mentorship. This work could not have been completed without the experimental assistance and advice from Dr. Jaehyung Park, Dr. Hongyan Ma and Dr. Hong Zhang. I am deeply indebted the entire Bryers lab for their valuable conversations, troubleshooting, and camaraderie. Finally, I would like to thank my family and friends for all their love and encouragement throughout my graduate tenure.

Chapter 1 Introduction

1. Statement of problem

Dendritic cells (DCs), as one type of potent antigen presenting cells (APCs), can activate T cells very efficiently (Banchereau J, 1998). Compared to vaccine developed from protein/peptide, which were usually weak stimulators of CD8+ T cells and Th1-type T cells, DC targeting nucleic acid vaccines have the potential to activate both CD4- and CD8- bearing cells, eliciting balanced and sustained humoral and cellular immune response.

In vivo targeting and activation are two major challenges facing the development of DC vaccines. This is because there is a low number circulating DCs *in vivo* and their activation requires both antigen uptake and a microenvironment with proper cytokine/chemokine stimulations. Early DCs based vaccines required cell isolations and programming *ex vivo* followed by transplantation back to patients. This process is time and resource consuming as well as inefficient (Kleindienst & Brocker, 2003). Most efforts in the delivery of nucleic acids vaccines *in vivo* involved bolus delivery of gene contained nano- or micro- particles targeting DCs (Palucka & Banchereau, 2012). Responses induced by such systemic bolus delivery is usually transient and limited for a lack of sufficient exposure to antigens, and a proper microenvironment for cell activation. These results necessitate the development of a validated vaccine platform that facilitates efficient delivery and supports cell activation *in vivo*.

This thesis proposes a novel way to use porous scaffolds as a local gene delivery vehicle to promote dendritic cell activation and to facilitate mRNA delivery *in vitro* and *in vivo*.

2. Hypothesis and research objectives

The hypothesis for this work states that: Implantable porous polymer scaffolds of certain materials and pore sizes can improve immune cell recruitment and maturation. By delivering mRNA therapeutics from these implanted scaffolds, cells recruited to the implant will have prolonged exposure to antigens and the proper microenvironment for activation, which eventually leads to improved APC transfection and more robust immune response compared to conventional bolus delivery methods.

The goal of this work was to develop a porous polymer scaffold platform as a novel strategy for mRNA vaccine local delivery. Poly (2-hydroxyethyl methacrylate) (pHEMA) and poly (dimethylsiloxane) (PDMS) scaffolds of various pore sizes were fabricated and their ability to activate dendritic cells were examined *in vitro* and *in vivo*. The optimal scaffold design was then combined with reporter mRNA to evaluate cellular uptake and expression *in vitro* and *in vivo*. The specific aims for this research were as follows:

Specific Aim 1: Fabricate and characterize porous polymer scaffolds. Using two types of biomaterials of differing chemistry, pHEMA and PDMS, fabricate porous scaffolds with three distinct pore sizes (20 μm, 40 μm, 90 μm) using a patented sphere-templating methods. Verify the physical porous structure characteristics of the various scaffolds.

Specific Aim 2: Characterize the interactions between dendritic cells and biomaterials *in vitro* and *in vivo*. Assess *in vitro* and *in vivo*, the cell response to scaffolds fabricated in Specific Aim 1. To determine DCs maturation state, pro-inflammatory cytokines and chemokines released

into supernatant by DCs will be measured, along with the assessment of cell bound maturation markers and co-stimulatory molecules. Quantify the ability of the various scaffolds to recruit and activate DCs in an *in vivo* mouse model. Evaluate scaffolds adjuvant effect to promote humoral and cellular immune response, using antigen ovalbumin (OVA) co-delivered with scaffolds.

Specific Aim 3: Quantify the efficacy of porous scaffolds as a local gene delivery device for reporter mRNA vaccine vectors. A series of transfecting reagents and cells will be screened *in vitro* to optimize mRNA transfection to APCs. Different surface modifications and loading strategies will be optimized for higher loading efficiency. Finally, the complete scaffold: nucleic acid vector system was evaluated *in vitro* and *in vivo* for mRNA retention, cell uptake, and gene expression.

Chapter 2 Background

1. Dendritic cell activation and immune therapy

1.1 DC immunology

The human immune system consists of innate and adaptive immunity. Innate immunity can identify common structures present on many microorganisms and protect the host from pathogens, while adaptive immunity is the response of antigen-specific lymphocytes to a specific antigen present on a pathogen. Adaptive immunity also controls the development of immunological memory. Dendritic cells (DCs) are the crucial link between these two immune responses. DCs are known to be the only type of antigen presenting cell (APC) that can prime T cells and initiate adaptive immunity. DCs usually reside in most tissues where they remain in an "immature" state, that is characterized by limited mobility, high endocytic ability, high intracellular MHC-II, and low co-stimulatory molecule expression (Banchereau J, 1998). During pathogen invasion and inflammation, DCs can recognize common non-specific repetitive structures existing in microorganisms termed "pathogen-associated molecular patterns" (PAMPs) by various pattern recognition receptors (PRRs) on the DC cell surfaces; such as toll-like receptors (TLRs). PAMPs signals combined with cytokine stimuli will activate DCs, promoting antigen uptake and maturation. The maturation process can be greatly influenced and shaped by factors present within the microenvironment, notably cytokines and chemokines, such as GM-CSF, IL-4, TNF-α, IL-10 (Rutella, Danese, & Leone, 2006). Upon maturation, DCs will increase motility to migrate to lymphoid tissues. A fully activated DC will present antigen fragments through the surface MHC class-II or MHC class-I complexes and express co-stimulatory molecules such as CD80 and CD86. With these two signals and cytokine cues, DCs can activate T lymphocytes and direct their

polarization. IL-12 secreted by DCs is dominant in the development of T_H1 cells that produce high amounts of IFN-γ (Moser & Murphy, 2000). In contrast, IL-10 is likely to induce a tolerogenic T_H2 response that produces IL-4 (Kapsenberg, 2003). DCs are the most potent and efficient APCs in the body. Only one activated DC is necessary to stimulate 100 – 3000 T cells (Banchereau J, 1998).

1.2 DC targeting immunotherapies

DCs central role in immunity makes them very attractive target for immunotherapies that aim to modulate the body's immune response. In the past two decades, significant progress has been made in the field of cancer immunotherapy, which aims to induce tumor-specific effector T cells (Palucka & Banchereau, 2012). Early attempts consisted of culturing DCs *ex vivo* with tumor specific antigens and adjuvants, then transplanting DCs back to the patients. Sipuleucel - T (Provenge) was a therapeutic that targets metastatic prostate cancer that demonstrated a 4-month-prolonged median survival in Phase III clinical trials (Sandham et al., 2010). Provenge became the first US Food and Drug Administration (FDA) approved prostate immunotherapy in 2010. However, high cost, low cell viability (<10%) and low lymph node homing (~0.5-2%) remain to be problematic with *ex vivo* therapies (Kleindienst & Brocker, 2003). Consequently, more research groups are turning to *in vivo* DCs modulations. It is usually achieved by delivering antigens with selected adjuvant to promote DCs targeting and activation (Bonifaz et al., 2004). The challenge will be to match the DC surface target and the selected adjuvant with the sustained immune outcome. So far efficacy has been demonstrated in many models with both viral and non-viral based approaches (Breckpot, Aerts, & Thielemans, 2007; Mograo, Da Costa, Gaspar, & Florindo, 2016).

2. DCs modulation with biomaterials

2.1 Mechanism of DC interaction with biomaterials

In the fields of tissue engineering and vaccine delivery, biomaterials are often used in combination with biological components to improve tissue regeneration or drug stability. The study of DCs response to biomaterials began in the context of learning the immune response associated with biomaterials adjuvant effects (Babensee, 2008). Biomaterial components recruit APCs and induce their activation, thus acting as an adjuvant to stimulate the immune response (Matzelle & Babensee, 2004).

Babensee's group identified TLRs and integrins as the key factors contributing to DC interaction with biomaterials. They hypothesized that DCs interact with materials in a contact dependent manner similar to their recognition of pathogens (Acharya, Dolgova, Clare-Salzler, & Keselowsky, 2008). Biomaterial surface structures, and proteins and other danger signals adsorbed onto the biomaterials are recognized by the PRRs; primarily C-type lectin receptors (CLRs); and Toll-like receptors (TLRs) (especially TLR2, 4, 6)(Reddy, Swartz, & Hubbell, 2006; Shokouhi et al., 2010). Physical structure can induce conformational changes and DC activation through integrin receptors. Previous studies suggested that higher hydrophobicity correlated with higher DCs maturation (Kou, Schwartz, Boyan, & Babensee, 2011; Park & Babensee, 2012), possibly because these materials mimic the hydrophobic domains of PAMPs (Reddy et al., 2006). Similarly, some natural materials with surfaces that contain carbohydrate structures are more likely to induce DCs maturation (Park & Babensee, 2012).

Consequently, biomaterials can be applied to promote or inhibit DCs maturation. For example, DCs treated with PLGA and chitosan showed higher levels of maturation, agarose and alginate induced similar levels of maturation as immature DCs (iDCs), while hyaluronic acid film inhibited maturation (Babensee & Paranjpe, 2005). Such modulation of DCs by biomaterials can also skew the adaptive immune response towards T_H1 (Acharya et al., 2008) or T_H2 type (Matzelle & Babensee, 2004) responses.

2.2 DC interaction with 3D scaffolds

Most of the early studies of DC interaction with biomaterials were limited to solid films or solid nanoparticles. Bennewitz *et al*. demonstrated that solid scaffolds induced higher humoral response compared to microparticles made out of the same material when co-delivered with the same antigen (Bennewitz & Babensee, 2005). As many of the scaffold based gene delivery applications have demonstrated success in promoting immune response *in vivo*, there have also been some studies exploring the relationship between DC activation and 3D porous scaffolds, particularly within the context of DC recruitment (Kim, Li, Sands, & Mooney, 2014; Leifer, 2017; Li et al., 2016). Li *et al*. demonstrated enhanced immune cell adhesion and infiltration by modulating the surface chemistry of mesoporous silica micro-rod (MSR) scaffolds with the integrin-binding ligand Arg-Gly-Asp (RGD) (Li et al., 2016). Lower surface porosity was correlated with higher infiltration *in vivo* due to better mechanical strength (Kim et al., 2014). It was also reported in the same study that scaffolds with pore sizes ranging from 10-1000 μm lead to similar level of DCs recruitment. While most of these studies focused on DC infiltration and migration in the porous scaffolds, how DCs are activated by porous structures has not been considered. Most of our knowledge is based on macrophage interaction with porous scaffolds in the context of wound

healing. Templated porous scaffolds with 38 μm pores were found to be optimal for vascularization and tissue integration, while larger pores (>200 μm) led to low vascularity and promoted cartilage tissue formation (A. Marshall et al., 2004; Matsiko, Gleeson, & O'Brien, 2015). It was later found that such angiogenesis induced by 38μm pore size coincided with a shift in macrophage phenotype toward the anti-inflammatory M2 state (Madden et al., 2010). While macrophages and DCs share the same precursor and both are antigen presenting cells, a study by Oliveira et. al. demonstrated that chitosan promotes anti-inflammatory phenotype in macrophages while DC display pro-inflammatory features (Oliveira, Santos, Oliveira, Torres, & Barbosa, 2012).

3. Scaffold mediated gene delivery

Porous scaffolds can be used to achieve sustained release of multiple factors, while providing a temporary residence and appropriate microenvironment for cell interaction (Xie, Yang, & Kniss, 2001). Compared to bolus delivery method, scaffold mediated gene delivery exhibited similar to or greater expression with orders of magnitude less DNA (Jang, Bengali, Houchin, & Shea, 2006). Different forms of scaffolds and non-viral gene vectors have been developed to facilitate the immobilization, release, and uptake of gene therapeutics (O'Rorke et al., 2010). In immunotherapy applications, the design of biomaterial scaffolds needs to be refined to better suit the different goals of immune response modulation. While scaffolds are usually designed to promote tissue regeneration and to minimize inflammatory response in tissue engineering applications, those may not be the design criteria for vaccine applications. Research groups have released chemokines from scaffolds to recruit iDCs and other immune cells (Shea, Smiley, Bonadio, & Mooney, 1999; Stachowiak & Irvine, 2008), demonstrating the potential to regulate DCs trafficking and activation *in situ* with scaffolds. Mooney and colleagues developed a poly(lactide-co-glycolide) scaffold

based cancer vaccine that consists of GM-CSF, tumor lysate (B16 melanoma), and CpG-ODN (O. A. Ali & Mooney, 2008). It showed promising results in animal trials (O. a Ali, Huebsch, Cao, Dranoff, & Mooney, 2009) and began phase I of clinical trials in 2012 as the first scaffold based cancer therapeutics.

4. RNA gene delivery

4.1 RNA vaccine

Wolff *et al*. (Wolff et al., 1990) first demonstrated in 1990 mRNA and pDNA induced protein expression in skeletal muscle followed shortly thereafter by the demonstration that nucleic acids could promote immune responses to encoded antigens (Ulmer et al., 1993). This opened a new avenue for numerous innovations in gene therapies.

Many features of mRNA make it a very attractive candidate for vaccine and immunotherapy development. First of all, mRNA has a superior safety profile over viral vectors and DNA. The genetic information carried by mRNA will be processed and expressed in cytoplasm without the need to enter the nucleus. So mRNA expression is transient and there is no risk of genomic integration. Because there is no need to cross nuclear membrane, mRNA is much more efficient at transfecting quiescent cells, many of which are the target cells for gene therapies and vaccines including hepatocytes and dendritic cells. As vaccines, mRNA also serves as its own adjuvant at the same time through activation of toll-like receptors (TLR) 7/8 and 3 (Alexopoulou, Czopik Holt, Medzhitov, & Flavell, 2001; Diebold, Kaisho, Hemmi, Akira, & Sousa, 2004; Heil et al., 2004). This is significant because it enables mRNA to trigger both arms of the humoral and cellular immunity, triggering balanced and robust immune response. Last but not the least, mRNA

customization and manufacturing can be easily achieved at a low cost via *in vitro* transcription. This allows for personalized treatments as well as rapid development of new vaccines during pandemics.

Although the proof of concept for RNA's use in vaccination was demonstrated decades ago, mRNA has long been considered not suitable for therapeutics mainly because it is easily degraded by various enzymes *in vivo*. In recent years, as many biomaterials based technologies were developed to improve stability and to facilitate transfection, *in vivo* mRNA application has regained traction. Research efforts have been mostly focused on cancer immunotherapies as evidenced by a large number of nonclinical and clinical studies (Kreiter, Diken, Selmi, Türeci, & Sahin, 2011).

Self-replicating RNA (sr-mRNA), also known as self-amplifying RNA or RNA replicon, is a class of mRNA developed to combine the advantages of mRNA and viral based vectors. It's derived from RNA viruses with the structural protein genes replaced with gene of interest. They are capable of amplifying the genes for prolonged period of time without producing infectious progeny. As mRNA, sr-mRNA are also effective at eliciting both humoral and cellular immune responses (Geall, Mandl, & Ulmer, 2013). Their potency have been demonstrated in various animal models and humans (Bernstein et al., 2009; Carroll et al., 2011).

4.2 Carriers for mRNA delivery

Multiple studies have reported that naked mRNAs exhibit poor ability to transfect cells and have very short half-life *in vivo* (Phua, Leong, & Nair, 2013). The enzymatic liability poses a great barrier for the development of mRNA therapeutics. Strategies have been developed to condense

anionic nucleic acids with various cationic lipids and polymers, which helps stabilize nucleic acids while facilitating the endosomal escape process. While poly (ethylenimine) (PEI) has been considered one of the most efficient polymers for gene delivery (Godbey, Wu, & Mikos, 1999), lipid based carriers have shown better capacity at facilitating mRNA transfection (Yamamoto, Kormann, Rosenecker, & Rudolph, 2008). It is hypothesized that lipids and polymers with smaller molecular weight have a weaker bonding strength to mRNA than large polymer molecules, facilitating the release of mRNA in cytoplasm, which is necessary for ribosome recognition and translation (Bettinger, Carlisle, Read, Ogris, & Seymour, 2001; Rejman, Tavernier, Bavarsad, Demeester, & De Smedt, 2010). Polymer carriers have also been decorated with specific cell binding peptides to improve DC targeting *in vivo* (Moffatt & Cristiano, 2006). More recently, systems combining both lipid and polymer components, such as lipoplyplex and lipid nanoparticles, have shown promise in optimizing both transfection efficiency while lowering cytotoxicity (Persano et al., 2017; Su, Fricke, Kavanagh, & Irvine, 2011).

Chapter 3 Scaffolds fabrication and *in vitro* characterization of dendritic cell response

1. Introduction

An ideal biomaterial scaffold for local vaccine delivery application should be able to 1) promote DC phenotype that favors antigen uptake and subsequent lymph node homing; 2) support cell infiltration and migration *in vivo* for access to therapeutics delivered and exit to draining lymph node; and 3) demonstrate good biocompatibility and induce minimal fibrous encapsulation for sustained delivery.

In previous studies, we fabricated scaffolds with controlled, monodisperse pore sizes and explored their impact on cell differentiation and tissue integration. 30-40 μm pore diameter were found to be optimal for vascularization and tissue integration, while larger pores (>200 μm) led to low vascularity and promoted cartilage tissue formation (Galperin et al., 2013). It was later found that such angiogenesis induced by 30-40 μm pore size coincided with a shift in macrophage phenotype toward what has been termed as an anti-inflammatory M2-state (Madden et al., 2010). Therefore, we hypothesize that pore size could also play a significant role in dendritic cell activation. To study how DCs maturation in scaffolds is impacted by material surface and pore structures, poly (2-hydroxyethyl methacrylate) (pHEMA) and poly (dimethylsiloxane) (PDMS, silicone) were fabricated into a series of scaffolds with uniform pore sizes. pHEMA and PDMS are two common synthetic polymers widely used in tissue engineering and drug delivery applications. Both are biocompatible and have high mechanical strength, which makes them suitable for implantation. pHEMA is a hydrogel with good permeability. PDMS is relatively hydrophobic and adsorbs

proteins which are reported to promote DCs activation (Park & Babensee, 2012). PDMS induced macrophage activation has also been previously reported (Iribarren, Correa, Sodero, & Riera, 2002).

All the scaffolds in this study were fabricated using the sphere-templating method that generates uniform and interconnected pores with controllable pore size (A. J. Marshall & Ratner, 2005). Scaffolds of 3 pore sizes (20 μm, 40 μm, 90 μm) were constructed. Scanning Electron Microscopy (SEM) was used to characterize scaffolds' morphology as well as determine pore sizes. A metabolic assay (XTT) as well as LIVE/DEAD® stain were used in combination to study cell viability in the 3D structures.

Scaffold ability to promote DCs maturation was evaluated *in vitro* with JAWsII murine dendritic cell line. DCs maturation is characterized by dramatic cell conformational changes. This process is also accompanied by increased secretion of pro-inflammatory cytokines, chemokines, higher expression of surface MHC-II molecules and co-stimulatory molecules. JAWsII cells were seeded into scaffolds and cultured for 24-48 h. Cytokines (TNF-α, IL-6, IL-10, IL-12), chemokine (RANTES, MIP-1α) released into the supernatant by DCs were measured. Up-regulation of surface markers CD80, CD86 and MHC-II on DCs surface was quantified by flow cytometry. Additionally, two-photon microscopy was used to validate the findings non-invasively *in situ*, namely DCs infiltration and CD86 expression after 48 hours.

2. Experimental methods

2.1 Scaffold fabrication

2.1.1 Sphere-templating method

Scaffolds with controllable and interconnected pores were fabricated using sphere-templating method (**Figure 3.1**) as described earlier (A. J. Marshall & Ratner, 2005). Poly (methyl methacrylate) (PMMA) beads were obtained from Microbeads AS (Norway) and Polysciences, Inc. (Warrington, PA) and sorted using an ATM Sonic model L3P Sifter (Milwaukee, WI) to obtain a particle size distribution reflecting the sieve mesh size required for each range. These sifted beads were poured into a 75 mm x 25 mm x 1 mm glass slide mold with 1 mm or 0.5 mm thick Teflon strips serving as spacers. Filled molds were sonicated for 30 minutes in a water bath sonicator to ensure good bead packing. Beads were sintered (melted at their contact points) at 170 ˚C (20 μm), 175 °C (40 μm) or 165 °C (90 μm) for 24 hours. Sintering procedure was optimized to obtain PMMA templates with neck sizes (interconnects between the beads) approximately 30% of the bead diameter. The template was then infiltrated with HEMA solution or PDMS gel for polymerization (details described below). After polymerization, the polymer/template sheet was removed from the glass mold or PTFE beaker and scraped with a clean razor blade to remove any nonporous film that may have formed between the scaffold and the mold. The scaffolds were washed in acetone for 72 hours with constant changes of solution to dissolve the PMMA template. Scaffolds were then cut to 3 mm discs using a biopsy punch and placed in 70% ethanol (3 x 1 hour) for sterilization. Ethanol was slowly exchanged for sterile PBS and samples were stored at 4 °C until experimentation. Scaffolds were evaluated for endotoxin using a standard limulis amebocyte lysate (LAL) gel clot protocol (Lonza). All scaffold batches used for *in vitro* and *in vivo* study contained endotoxin less than 0.06 EU/ml.

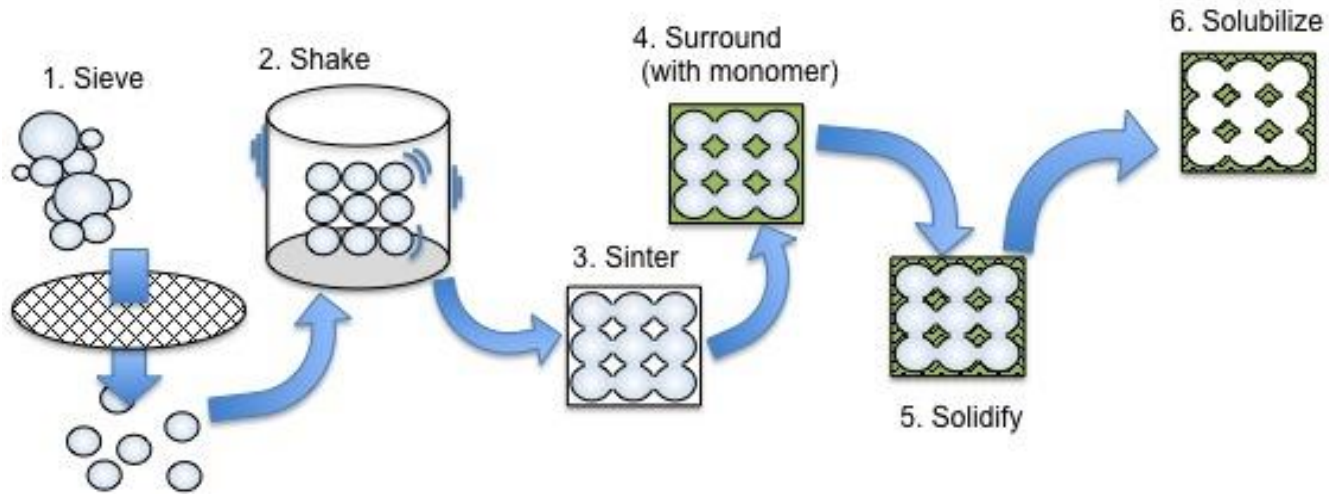

Figure 3.1 Illustration of scaffolds fabrication with sphere-templating method.

2.1.2 pHEMA polymerization

pHEMA precursor consisted of 5 mL 2-hydroxyethyl methacrylate (HEMA) (Polysciences), 0.23 mL tetraethyleneglycol dimethacrylate (TEGDMA) (Polysciences), 2.0 mL deionized water, 3.6 mL ethylene glycol, and 20 mg 2,2-dimethoxy-2-henylacetophenone (Irgacure 651) (BASF, Freeport, LA). The reaction mixture was then infiltrated into the glass mold surrounding the bead template and degassed under vacuum for 30 minutes. pHEMA hydrogel was polymerized under broad-spectrum UV from a high-intensity mercury lamp for 10 minutes by photo initiated free-radical copolymerization.

2.1.3 PDMS polymerization

Silicone gel components were obtained from Applied Silicone. Silicone base component vinyl terminated polydimethylsiloxane and crosslinker silica were thoroughly mixed in 10:1 ratio in advance. The mixture was then poured on top of the template inside of a PTFE beaker (Sigma-

Aldrich). Because of high viscosity (~100,000 cps) of the polymer, the beaker was centrifuged at 4000 rpm for 10 minutes to ensure thorough infiltration. Afterwards, the beaker was placed inside a vacuum chamber and degassed at 28" Hg for 1 hour. The polymer was then cured at 130 ˚C for 30 minutes.

2.2 Scanning electron microscopy (SEM) imaging

Scanning electron microscopy was performed on lyophilized scaffold samples to confirm that the dimensions of the scaffolds adhered to specifications. Lyophilized samples were sputter coated for 120s with gold/palladium in a sputter coater (~20nm layer). Scaffolds were then imaged on a scanning electron microscope (FEI SEM XL Siron) at 5 kV with a 5 mm working distance. Both cross-section and top view were observed. ImageJ software was used to measure the size of pores and interconnect pores based on the images collected from SEM. For each scaffold and template, 3 top-view images from different batches were analyzed and 10 sample points were measured from each image.

2.3 Cell culture

All cell culture media and reagents were obtained from Gibco unless otherwise specified. JAWsII murine dendritic cell line (ATCC) were maintained in alpha minimum essential medium (alpha-MEM) containing L-glutamine supplemented with 2 mM L-glutamine, 20% fetal bovine serum (FBS), 1% penicillin-streptomycin, and 10 ng/µl GM-CSF. All cells were cultured at 37 ˚C and 5% CO_2.

2.4 Cell viability in scaffolds

2.4.1 XTT assay

Scaffolds were punched into disks that fit inside non-treated 24-well tissue culture plates (NTPS) (Corning) and were pre-soaked in complete culture medium overnight prior to experiments. JAWsII cells were seeded onto the scaffolds in 24-well plates at 500,000 cells/well in 0.5 mL complete medium. Immature DCs (iDC) seeded directly on NTPS with medium only or lipopolysaccharide (LPS) stimulated DCs (mDCs) were used as controls. The plate was centrifuged at 1100 rpm for 5 minutes. After adding another 0.5 mL culture medium into each well, cells were cultured at 37˚C. After 24 h culture, supernatant was collected for XTT assay and total DNA content in each well was quantified using the CyQUANT^{TM} assay. To perform XTT assay, 50 µl of 1 mg/mL XTT (2,3-Bis-(2-Methoxy-4-Nitro-5-Sulfophenyl)-2H-Tetrazolium-5-carboxanilide) (Life Technologies) and 4 µL 1 mM menadione (Sigma-Aldrich) were added to each well. Extra blank wells were prepared containing the same amount of reagents and culture medium. Plates were gently mixed and covered with aluminum foil then incubated for 4 hours at 37 ˚C. The reaction mixture was then transferred into microcentrifuge tubes and centrifuge for 5 minutes to remove any cells in the suspension. 200 µL supernatant was taken from each sample and added into 96-well plate. Absorbance was measured at a wavelength of 492 nm using a Tecan Safire 2 microplate reader. Standard curve was obtained by measuring metabolic activity of a known number cells. All results were converted into viable cell numbers using the standard curve then normalized to same reading for cells cultured on NTPS.

2.4.2 LIVE/DEAD® stain

After 48 h culture, sc9affolds and cells were fixed with 2% BD Cyto-fix (BD Biosciences) for 15 minutes at room temperature. LIVE/DEAD® kit (Life technologies) was used to perform viability

assays. 2 μM calcein AM and 4 μM EthD-1 solution was mixed at 1:1 ratio. 100~150 μL of mixed stain reagents were added to the surface of the scaffold and incubated for 30~45 minutes at room temperature. Stained scaffolds were washed 3X with PBS and imaged with an Olympus FV1000 MPE BX61 multi-photon microscope.

2.5 Maturation cytokines and chemokines release

JAWsII cells were seeded onto NTPS or scaffolds in a 24-well plate at 500,000 cells/well density in 1 mL complete medium. Cells seeded on NTPS and stimulated with 100ng/mL lipopolysaccharide (LPS) were used as positive control for mDCs. After 24 h co-culture with biomaterial scaffolds, the cell culture supernatant was collected and centrifuged for 10 minutes to remove non-/loosely adherent cells in the suspension. Total DNA content in each well was quantified using CyQUANT assay. Supernatants were stored at -20˚C until analysis. The amount of tumor necrosis factor-α (TNF-α), IL-6, IL-12, IL-10 and chemokines RANTES and MIP-1α released by DCs into the supernatant after co-culturing with scaffolds were analyzed by ELISA according to the manufacturer's direction (Peprotech, NJ). Results were converted into viable cell numbers and normalized to the same parameter for cells cultured on NTPS.

2.6 Flow cytometry

After 24 h co-culture within biomaterial scaffolds, cells were collected by PBS-based cell dissociation buffer (Invitrogen) and resuspended in 200 μL FACS buffer (DPBS containing 2% FBS) at concentration 1,000,000 cells/mL. Nonspecific binding was blocked by incubating with anti Fcγ III/II receptor antibody (1:500) (BD Biosciences) at 4 ˚C for 5 minutes. FITC conjugated

CD86 antibody (Biolegend) was diluted 1:1000 and incubated with cells on ice in the dark for 30-40 minutes. Cells were washed twice with PBS and resuspended in 200 µL FACS buffer with 0.2 µg/mL propidium iodide (Invitrogen). To determine CD86 expression levels, 10,000 events per sample gated on viable propidium iodide-negative cells were acquired on a BD FACScan flow cyotometer (BD Biosciences) and analyzed using FlowJo software (TreeStar).

2.7 Two-photon microscopy

Two-photon microscopy was used to assess cells' infiltration into the scaffolds of varying pore sizes, as well as comparing cell maturation *in situ* in the depth z direction. JAWsII cells were seeded on 20 µm and 40 µm pHEMA scaffolds at 500,000 cells/well in 1 mL medium. After 48 hours incubation, samples were taken out and nucleic acids were stained by 1 µM SYTO-11 (Invitrogen) and/or CD86 (1:100, Biolegend) antibody. To reduce optical density for deeper imaging, samples were cleared with benzyl alcohol (BA) after fluorescent immunolabeling and mounted in BA in concavity slides for imaging. Multiphoton excitation microscopic images were captured using an Olympus FV1000 MPE multiphoton microscope equipped with a 25x SuperObjective (Olympus) and Mai Tai laser (Spectra Physics). Z-series stacks about 200 µm in depth were collected and images were processed using ImageJ. Each z-series (depth into scaffold) stack was then converted into a brightest point projection image and pixel intensities of nucleic acids and CD86 were collected and compared with the measure function.

3. Results

3.1 Scaffold characterization

pHEMA and PDMS scaffolds of all three sizes 20 µm, 40 µm, and 90 µm were fabricated as described. SEM analysis (**Figure 3.2**) shows that using the protocol described above, results in scaffolds with uniform and interconnected pores. The 20 µm scaffolds inner pore surface was rough (**Figure 3.2,C**) due to the fact that 20 µm beads themselves had uneven surfaces. All pHEMA and PDMS scaffolds maintained their 3D morphology well after dissolving the PMMA template. ImageJ was used to quantitatively characterize the pore size as well as throat sizes based on SEM images (**Table 3.1**). At least one sample of template and scaffold from each batch were tested. For each size, the pores were uniform with small pore size distribution (standard deviation < 3% of the pore size). The size of the throats ranged from 30% to 40% of the pore size.

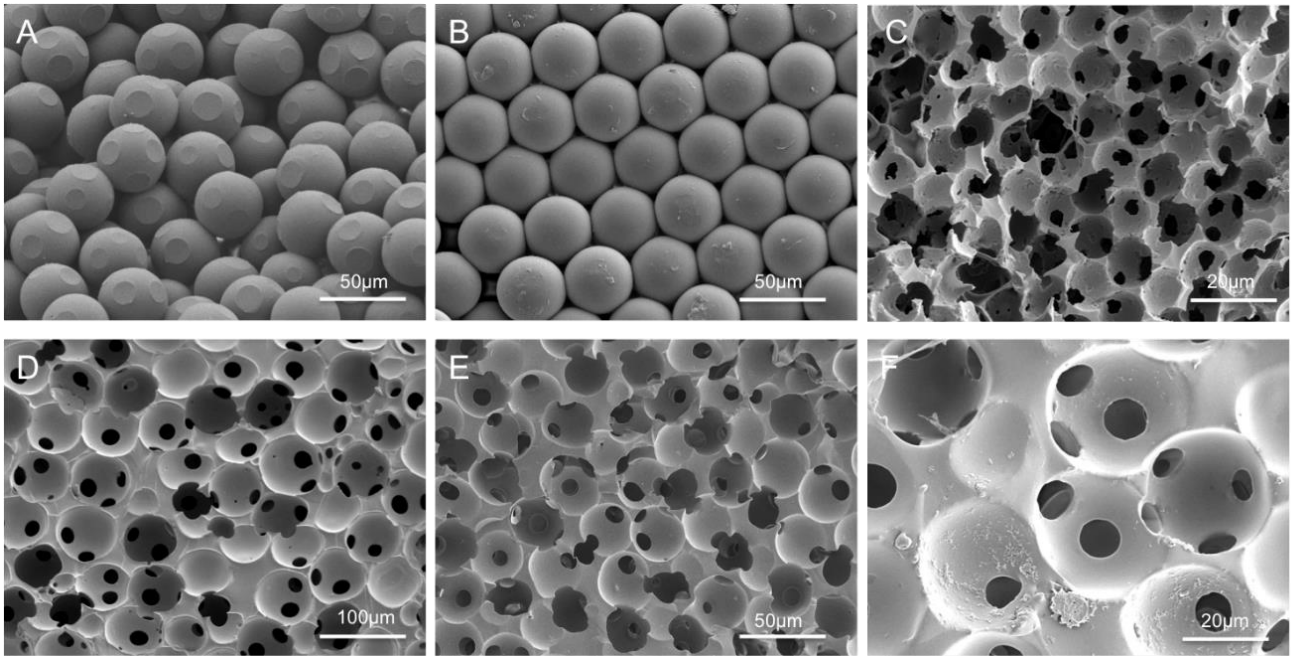

Figure 3.2 SEM images of sintered PMMA templates and scaffolds. (**A**) 40 µm template, cross-section; (**B**) 40 µm template, top view; (**C**) 20 µm pHEMA scaffold, cross-section; (**D**) 90 µm pHEMA scaffold, cross-section; (**E**) 40 µm pHEMA scaffold, cross-section; (**F**) 40 µm PDMS scaffold, cross-section.

Table 3.1 Pore size and throat size distribution. Values are calculated from SEM images analyzed with ImageJ. Results are displayed as means ± standard deviation.

Scaffold	Pore size (µm)	Throat size (µm)	Ratio (%)
Small	18.25 ± 0.36	5.45 ± 0.52	29.9 ± 2.87
Medium	38.75 ± 0.75	14.97 ± 0.75	38.6 ± 1.94
Large	92.10 ± 3.21	29.66 ± 1.46	32.2 ± 1.58

3.2 Cell viability

Cell viability was primarily determined by cell metabolic activities measured by the XTT assay and normalized by total DNA in each well. In LPS-treated negative controls, DCs viability decreased by half after 48 h culture (**Figure 3.3, top**) due to apoptosis of terminally differentiated DCs (Lu et al., 1996). All cells seeded into porous scaffold exhibited good viability that was equal to or higher than those cultured on NTPS surface. LIVE/DEAD® stain was used to confirm the results obtained from XTT assay. A majority of the cells in the field stained green indicating viable cells (**Figure 3.3, bottom**). Cells seeded on biomaterial scaffold have similar viability compared to the cells cultured on NTPS surfaces. Most cells showed round morphology, indicating an immature state. Significant amount of cell loss was noted in LPS treated samples due to loss of adhesion and apoptosis in terminally differentiated DCs.

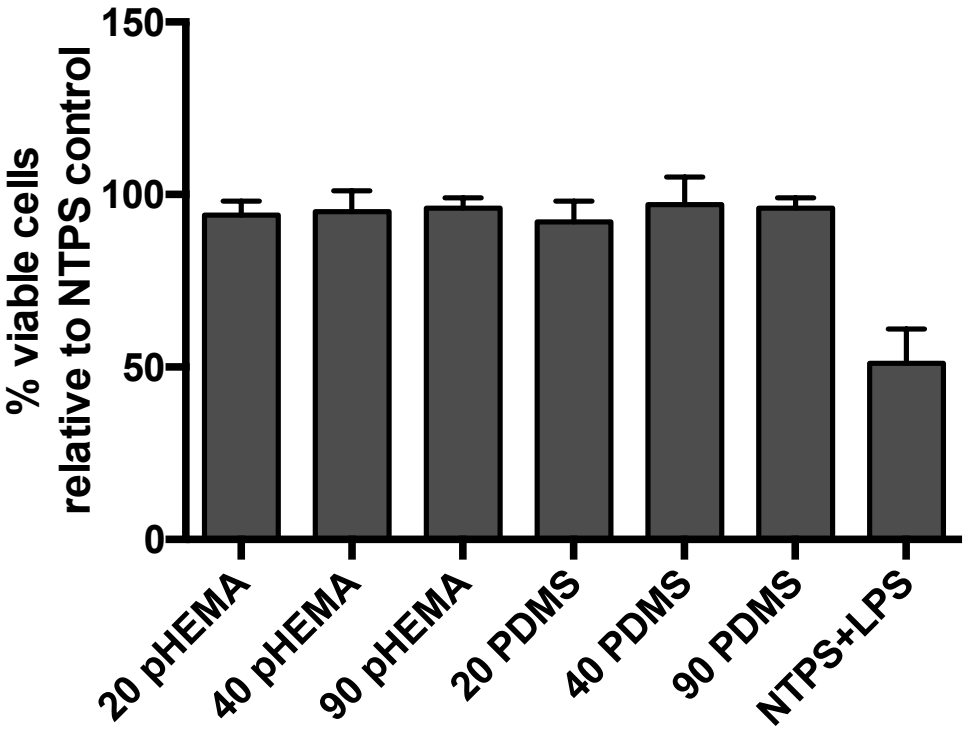

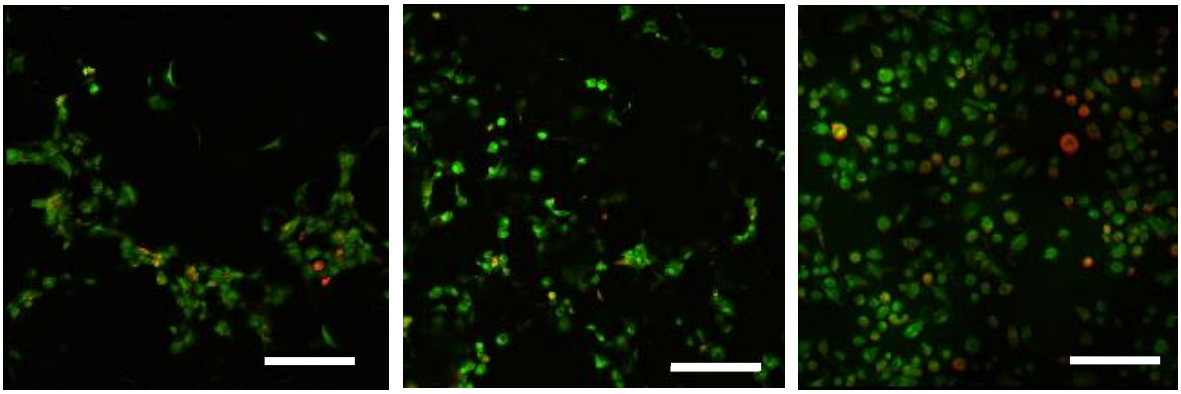

Figure 3.3 Cell viability within scaffolds. **Top**: Viable cells after 48 hours culture with biomaterial scaffolds measured by XTT assay. Data was normalized relative to cells cultured on NTPS. Results are from single representative experiment conducted in triplicate ± standard deviation. **Bottom**: Cells cultured on (**A**) 40µm pHEMA scaffold; (**B**) 40µm PDMS scaffold; and (**C**) NTPS for 48 hours. Live cells were stained with calcein AM (green) and dead cells with membrane damage were stained with EthD-1 (red). Scale bar = 100µm

3.3 Maturation cytokines and chemokines

Cytokine production kinetics by DCs stimulated with LPS suggested that TNF-α can be detected as early as 3-4 hrs and continues to increase until 10 hrs upon reaching a plateau. IL-6 secretion starts at 6 hrs and is sustained for 24 hrs. IL-12 begins after 10 hrs and quickly plateaus around 12-18 hrs. A preliminary 72-hr time course study was carried out that determined 24 hrs was sufficient to evaluate cytokine secretion caused by DCs maturation. LPS-treated DCs had strong up-regulation of all the cytokines tested in this study (**Figure 3.4**, **Table 3.2**). TNF-α is a pro-inflammatory cytokine and a key mediator in innate immunity. After exposure to all biomaterials, DCs secreted 15-57 times more TNF-α than DCs on NTPS. IL-6 is known for inducing T_H1 type immune phenotype; Il-6 expression on the various scaffolds ranged from 5-31 times the IL-6 expressed on NTPS. RANTES levels were only slightly elevated in scaffolds; ranging from 1.3 – 12 times that seen on NTPS. MIP-1α secretion ranged from 21-211 times higher than cells seeded on NTPS. The amount of TNF-α, MIP-1α and IL-6 quantified by ELISA varied among different experiments but the general trend remained the same; smaller pore size induced more DC response regardless of the material. Levels of IL-10 and IL-12 were also quantified and there were no statistical differences observed on scaffolds versus iDC controls.

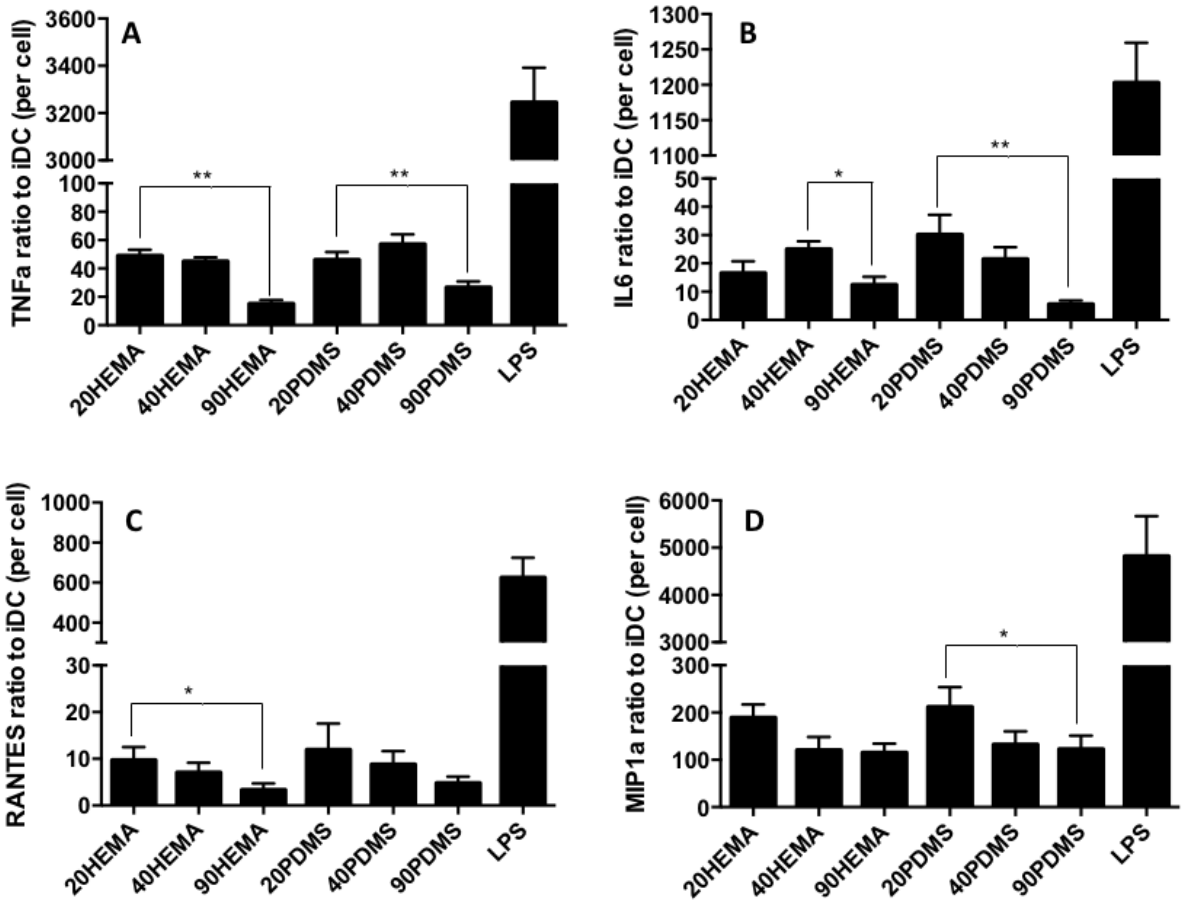

Figure 3.4 Supernatant analysis of maturation cytokines and chemokines. (**A**) TNF-α; (**B**) IL-6; (**C**) RANTES; (**D**) MIP-1α. Results are displayed in "per cell" expression relative to that of iDC on NTPS. All results are from single representative experiment performed in triplicate ± standard deviation. (* $p<0.05$, ** $p<0.01$)

Table 3.2 Cytokine Expression Levels (pg/10^6 cells)

	TNF-α	IL-6	RANTES	MIP-1α
IDC/NTPS	3.01	16.29	15.15	11.58
20HEMA	147.49	268.8848577	146.955	2181.652314
40HEMA	135.45	407.25	106.05	1389.6
90HEMA	45.15	201.996	49.995	1327.56015
20PDMS	138.46	490.837248	180.285	2449.79532
40PDMS	171.57	350.235	133.32	1529.215428
90PDMS	80.066	89.595	72.5685	1418.94951
LPS/NTPS	9765.945	19596.87	9474.123705	55774.42152

3.4 Flow cytometry of cell surface activation markers

Co-stimulatory molecule CD86 is expressed on JAWSII cell surfaces upon activation and is one crucial indication of DCs maturation. The percentage of DCs expressing CD86 was measured by flow cytometry and was normalized to the control group (iDCs on NTPS) at a 24-hr time point (<2%). After biomaterials culture or LPS treatment, all cells up-regulated CD86 and expression was increased progressively during maturation. At 24 hrs, CD86 expression on LPS-activated DCs (mDCs) was 5x higher than iDC on NTPS. DCs exposed to scaffolds increased CD86 expression 2~4 fold by 24-hr relative to iDCs on NTPS. Expression of CD86 surface markers decreased slightly with increasing scaffold pore size regardless of polymer (**Figure 3.5, A**). MHC-II surface markers for scaffold culture or LPS activated plate cultures were all ~1.3-2.0x higher than iDC expression. There appears to be little effect of pore size or construction of the polymer on MHC-II surface markers relative to iDCs. CD80 surface markers were all elevated for JAWSII cells cultivated on all scaffolds or in plates exposed to LPS; LPS activated cells were 43x higher than iDCs whereas scaffold cultivated JAWSII cell CD80 surface markers were 12-38x higher than iDCs, expression levels decreased with increasing pore size, independent of polymer (**Figure 3.5, C**).

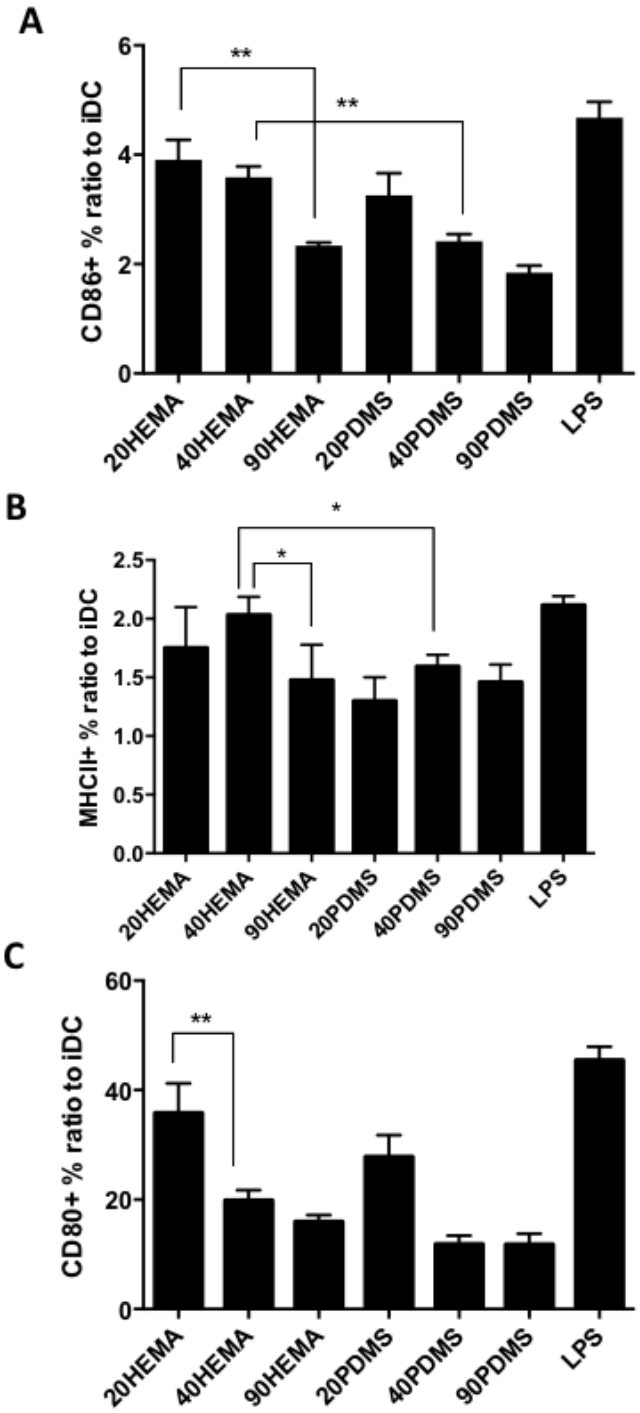

Figure 3.5 JAWSII cell surface marker expression levels for 24hr cultures within scaffolds. Cells were recovered from indicated polymer (pHEMA or PDMS) scaffolds as a function of scaffold pore size, relative to levels seen for iDCs on TCPS. JAWSII cells recovered from scaffolds were stained with antibodies to the indicated cell surface marker and detected by flow cytometry. (**A**) CD86, (**B**) MHC-II, and (**C**) CD80 expression relative to iDCs. All results are from single representative experiment performed in triplicate ± standard deviation. (* $p<0.05$, ** $p<0.01$)

3.5 Two-photon microscopy

Two-photon microscopy has been successfully applied to image thick tissue samples (Hartman, Reh, & Bermingham-McDonogh, 2010; Rice, Kaplan, & Georgakoudi, 2010). Clearing agents are used as a common procedure to match the refractive index (RI) of tissue samples and reduce optical density contrast for imaging. However, due to the difficulty to precisely determining the RI of 3D porous scaffolds, this method is not widely used for opaque polymer imaging. In this study, benzyl alcohol was discovered to clear opaque pHEMA scaffolds. Using this method, the imaging depth was increased from 50 to over 200μm in bright field which allowed 3D model reconstruction of the z-stack images in ImageJ to map scaffold cell distribution (**Figure 3.6**). Since PDMS materials cannot be visualized with the same clearing agent, only 20 and 40 μm pHEMA scaffolds were studied in this section as a proof-of-concept.

Cells seeded on 40 μm pHEMA scaffolds were able to infiltrate after 48 hours, while almost no cells were detected within 20 μm pHEMA scaffolds. Additionally, there was not a cell layer accumulating at the surface of pHEMA scaffold as we expected. This may be due to the fact that pHEMA is relatively hydrophilic and had limited protein adsorption within 48 hours. Most cells that had settled on the surface of the pHEMA scaffolds were lost during the repeated washing steps. Two-photon microscopy was also investigated for its potential to study cell phenotype *in situ* (**Figure 3.6**). After z-stack images were collected, the fluorescence intensities from images taken from close z-position were measured and compared. Setting the appropriate size threshold allowed each cell to be identified as one particle. Fluorescence intensity was measured for each particle. Nucleic acids stain intensity was used as a control. As seen in **Figure 3.6**, the DNA intensity from two images was approximately the same while CD86 (a DC marker indicating activation/maturation) showed a significant difference. Reasonable standard deviation was used as

an indication that cells within each treatment condition had a similar maturation pattern after 48 hours. However, due to the nonlinear signal attenuation from multiphoton microscopy, it was difficult to compare images taken from different z-positions. Additionally, the 0 position was determined manually which may have caused inaccuracy. In this study, the same method was applied to compare the maturation condition of the first 2-3 layers of cells and similar CD86 expression levels were found.

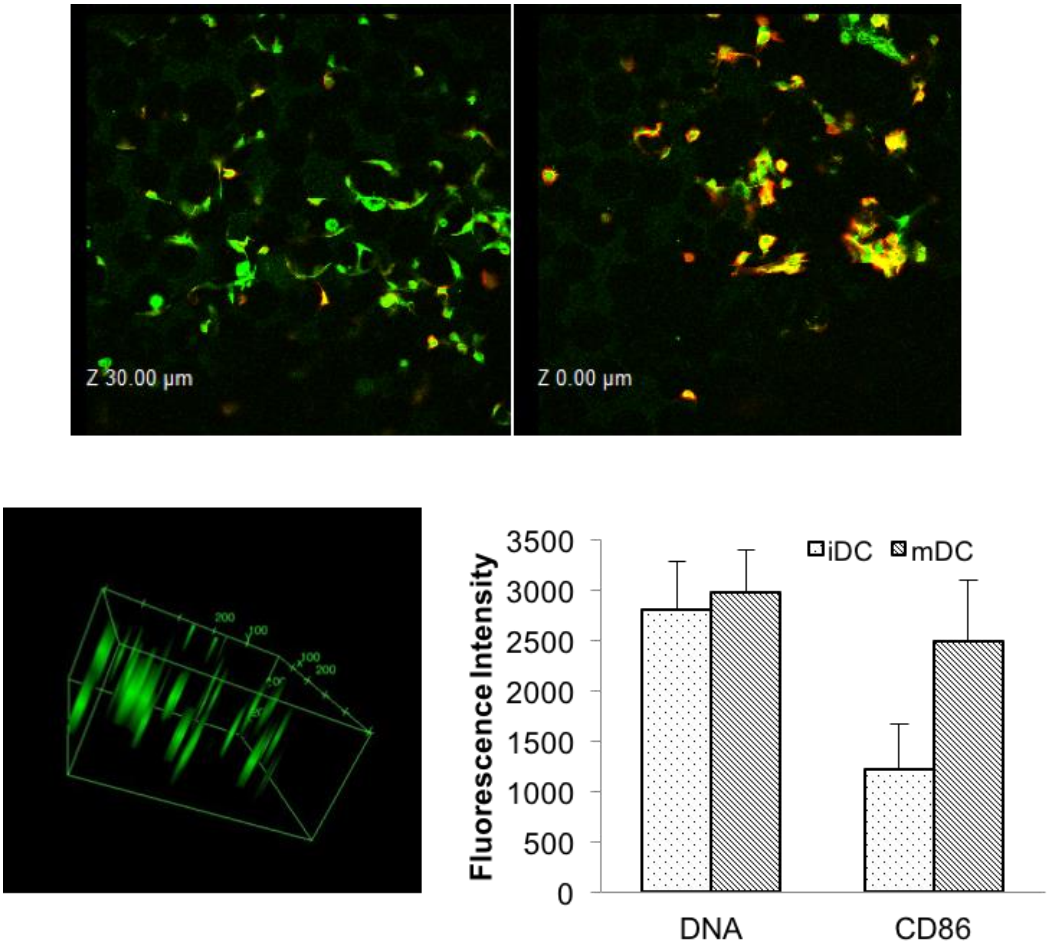

Figure 3.6 Two photon microscopy images (25x) of JAWsII seeded within scaffolds. **Top**: **left**, 40-µm pHEMA scaffold (iDC); **right**, 40-µm pHEMA scaffold treated with LPS (mDC). Nucleic acids were stained green and CD86 were stained red. **Bottom**: **left**, 3-D reconstruction of cell distribution in scaffolds; **right**, fluorescence intensity of each stain quantified by ImageJ.

4. Discussion

In this study, pHEMA and PDMS were selected because of their distinctive features and extensive use in tissue engineering applications. Hydrophilic pHEMA tends to prevent cellular adhesion and spreading and provides a substratum for cells that do not require anchorage to proliferate, thus promoting cell differentiation (Son et al., 2013). PDMS has multiple hydrophobic domains, which mimic PAMPs structures and has the potential to induce DCs activation, according to earlier studies (Babensee & Paranjpe, 2005). Aside from the type of biomaterial, we also explored how pore sizes may affect DCs maturation since reports suggest that scaffold pore size can affect cell migration, spreading, and differentiation (Galperin et al., 2013; Underwood et al., 2011). pHEMA and PDMS scaffolds were made with the sphere-templating method where every pore and interconnects are uniform in size, with both parameters being adjustable. Three pore sizes (20 μm, 40 μm, 90 μm) were chosen in this study to investigate the impact of pore size on DC maturation. SEM images and quantitative analysis confirmed the structural integrity of the scaffolds and the uniformity of the pore dimensions.

After co-culturing with JAWSII dendritic cell lines, all scaffolds to some degree induced a T_H1 type immune response as characterized by secretion of TNF- α, IL-6, RANTES, and MIP-1α (Banerjee, Biswas, & Biswas, 2008; Caux et al., 2002; Dieu-Nosjean, Vicari, Lebecque, & Caux, 1999; Sallusto et al., 1998). We expected and observed no detectable amounts of IL-10 in any group, since its up-regulation is an indication of an anti-inflammatory response(Corinti, Albanesi, la Sala, Pastore, & Girolomoni, 2001). Scaffolds with smaller pore sizes (20, 40μm) induced more secretion of T_H1 type cytokines and chemokines. This trend is consistent with the DC activation characterized by upregulation of MHCII and CD86 surface markers. When selecting vaccine adjuvants, a stronger APC activating ability is usually preferred to promote antigen uptake.

While simultaneous activation and antigen uptake do not always happen, such an occurrence could reduce overall antigen uptake and vaccine efficacy (Heit, Busch, Wagner, & Schmitz, 2008). It has been reported that fully activated DCs have lower endocytic ability and lower antigen presentation (Park, Wu, & Bryers, 2013; Platt et al., 2010). Stimulating signals such as LPS or CpG oligonucleotides can trigger DCs differentiation and eventually lead to cell apoptosis through CD14 (Zanoni et al., 2009). These findings suggest that when selecting an adjuvant for antigen delivery, it is important to match DCs activation kinetics with antigen release/uptake kinetics for optimal antigen uptake. While scaffolds with smaller pore sizes induced stronger T_H1 type response in DCs, their ability to promote immune cell recruitment and antigen uptake still needs to be demonstrated *in vivo*.

In this section we also described improved methods with which to study cell dynamics within 3D scaffolds. Cell viability is an important criterion of tissue engineering products. Most of the commonly used viability methods have been optimized for analysis of cells on 2-D surfaces. A few methods have been optimized for measuring cell viability inside of scaffolds, including the Alamar Blue and the MTT assays. While Alamar Blue is convenient for live cell imaging, scaffolds remaining in the solution tend to auto-fluoresce, thus interfering with readings. The MTT assay on the other hand requires an extra handling step that makes the procedure less accurate. In contrast, the XTT reagent is converted by viable cells to a water-soluble colored formazan product that can be easily extracted from the scaffolds. Results from different experiments were consistent and therefore the XTT method was considered as an effective way to measure the viabilities of cells growing within the scaffolds. Studying cells phenotype in a 3D structure can be challenging.

The potential of using two-photon microscopy to study cell phenotype in situ was explored in this section. Two-photon technology has been successfully applied to image thick tissue samples

(Hartman et al., 2010; Rice et al., 2010). In this study, benzyl alcohol was discovered to render opaque pHEMA scaffolds transparent, making it possible to image otherwise opaque polymer material. Using this method, the imaging depth was increased from 50 μm to over 200 μm in bright field. This remains a need to develop an imaging protocol to quantitatively compare fluorescent signals with depth into a specimen.

5. Conclusion

In this section, scaffolds of 3 pore sizes 20 μm, 40 μm, and 90 μm were successfully fabricated with two materials pHEMA and PDMS. SEM and ImageJ analysis proved that the dimensions of the scaffolds adhered to specifications. XTT assay and LIVE/DEAD® staining of cells seeded within scaffolds demonstrated that both scaffolds had minimal cytotoxicity.

JAWsII murine dendritic cell line was used to study DC response to the scaffolds. Secretion of pro-inflammatory cytokines TNF- α, IL-6, chemokine RANTES and MIP-1α was observed from all pore size scaffolds regardless of polymer. This was accompanied by upregulated expression of surface maturation markers CD86 and MHCII. Smaller pore sizes (20 and 40 μm) elicited higher pro-inflammatory response, in both pHEMA and PDMS scaffolds. These findings suggest that both pHEMA and PDMS can promote DC maturation and induce T_H1 skewed response. Smaller pore size (20, 40 μm) are more favorable for DC maturation regardless of the materials used.

Chapter 4 Evaluation of immune response to porous scaffolds *in vivo*

1. Introduction

Scaffolds structure and pore sizes are important parameters determining DC infiltration into the implants. Li *et al*. demonstrated enhance immune cell adhesion and infiltration through modulating surface chemistry of mesoporous silica micro-rod(MSR) scaffolds with the integrin-binding ligand, Arg-Gly-Asp (RGD) (Li et al., 2016). Lower surface porosity was correlated with higher infiltration *in vivo* due to better mechanical strength (Kim et al., 2014). It was also reported in the same study that scaffolds with pore sizes ranging from 10-1000 μm made no significant difference in the number of DCs recruited. While most of these studies focused on DC infiltration and migration in the porous scaffolds, porous structure effects on DC activation were not considered. Most of our knowledge is based on macrophage interaction with porous scaffolds in the context of wound healing. Scaffolds with 38 μm pores were found to be optimal for vascularization and tissue integration, while larger pores (>200 μm) led to low vascularity and promoted cartilage tissue formation (A. Marshall et al., 2004; Matsiko et al., 2015). It was later found that such angiogenesis induced by 38μm pore size coincided with a shift in macrophage phenotype toward the anti-inflammatory M2 state (Madden et al., 2010). While macrophages and DCs share the same precursor cell line and both are antigen presenting cells, a study by Oliveira *et al*. demonstrated that chitosan promotes anti-inflammatory phenotype in macrophages while DC display pro-inflammatory features (Oliveira et al., 2012).

In this section, pHEMA and PDMS scaffolds of three pore sizes were implanted in C578L/6J mice and evaluated for their abilities to recruit immune cells and promote DC maturation locally. The biomaterials adjuvant effect was also evaluated with co-delivery of model antigen ovalbumin (OVA) with 40 μm and 90 μm pHEMA and PDMS scaffolds. Serum anti-OVA IgG was measured as an indication for humoral response, while IFN-γ and IL-4 released by re-stimulated splenocytes were measured to evaluated cellular response.

2. Experimental methods

2.1 Scaffold implantation

All animal experiments adhered to federal guidelines and were approved by the University of Washington Animal Care and Use Committee. Groups of C578L/6J female mice (Jackson Laboratory, 6 to 8 weeks old; 3-5 mice per group) were used for this study.

pHEMA and PDMS scaffolds with 3 distinct pore sizes (20 μm, 40 μm, 90 μm) were used in this study. On Day 0, individual pHEMA or PDMS scaffolds were implanted subcutaneously in the dorsa of selected C57BL/6J mice. Briefly, mice were anesthetized and a 1 cm incision was made on the central dorsal surface. A subcutaneous pocket was made on either side of the incision, the biomaterial scaffold (3 mm diameter disk, 1 mm thick) was inserted, and the incision was closed with surgical clips.

2.2 Cell infiltration and distribution

After euthanasia, the implant and a 2-mm area of full thickness dermal tissue around the implant were excised together and fixed in 4% paraformaldehyde for 24 hours. After gradually replacing the PBS buffer with 30% sucrose solution, tissue was mounted in optimal cutting temperature compound (OCT) and frozen at -20 ˚C. Samples were kept at -80 ˚C until cryosection. OCT-embedded tissue was cut into 5-µm sections and stained with DAPI to visualize cell distribution.

Some samples were analyzed with SEM. Upon fixation, scaffolds were critical point freeze dried then cleaved into sections prior to gold/palladium sputter coating. The cross-sections of the scaffolds were then imaged on a scanning electron microscope (FEI SEM XL Siron) at 5 kV with a 5 mm working distance.

2.3 Immune cell recruitment and phenotype characterization

To assess cell recruitment and phenotype, scaffolds were excised at various time points, and the ingrown tissue was digested into single cell suspensions using a collagenase solution (Worthington, 250 U/mL) that was agitated at 37 ˚C for 45min. The cell suspensions were then poured through a 40 µm cell strainer to isolate cells from scaffold debris. Cells were then stained with primary antibodies conjugated to fluorescent markers to allow for analysis by flow cytometry.

2.4 Ovalbumin immunization

The study was designed as follows: 1. OVA only (OVA); 2. PBS only (PBS); 3. 40 µm pHEMA scaffolds only (40 pHEMA); 4. 40 µm PDMS scaffolds only (40 PDMS); 5. 40 pHEMA + OVA;

6. 40 PDMS + OVA; 7. 90 pHEMA + OVA; 8. 90 PDMS + OVA. Groups 1 through 4 were used as controls.

On day 0, pHEMA and PDMS scaffolds were implanted subcutaneously in the dorsa of selected C578L/6J mice. Briefly, mice were anesthetized and a small incision was made on the central dorsal surface. A small subcutaneous pocket was made on either side of the incision, biomaterial scaffolds (3 mm diameter disks, 1 mm thick) were inserted, and the incision was closed with clips.

For immunization, each mouse received 50 µL of sterile PBS or 50 µg OVA in 50 µL PBS solution (OVA) by subcutaneous injection on the back. For mice with implants, OVA solution was injected onto the scaffolds. Mice were immunized 3 times at 1-week intervals and euthanized 1 week after the last immunization, at which time spleens were harvested and scaffolds were explanted (**Figure 4.1**). Blood samples were collected each week 2 days prior to immunization via submandibular vein bleeds. Serum samples were prepared from the blood samples after clotting at room temperature for 4 hours and stored at -20 ˚C until antibody were evaluated by ELISA.

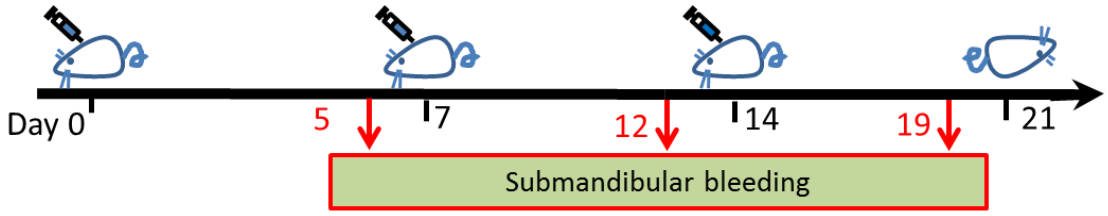

Figure 4.1 Immunization and sample collection schedule.

2.5 Serum OVA-specific antibody by ELISA

The production of anti-OVA total IgG in mouse serum sample was measured by ELISA. Standard 96-well Nunc Immuno MaxiSorp ELISA plates (Thermo) were coated overnight with 100µl/well

coating buffer (10µg/ml OVA (Invivogen) in PBS, 0.1% [w/v] sodium azide (Sigma)) at 4˚C. Plates were washed 4 times with 300 µl/well wash buffer (0.02% [v/v]) Tween 20 in PBS) in between each step. The plates were blocked with 15µl/well block buffer (1% [w/v] BSA in PBS, 0.22µm filtered) for 1 hour at room temperature. 100 µl/well of diluted serum samples in block buffer were then added to the plates and incubated at room temperature for 2 hours. 100µl/well secondary antibody [goat anti-mouse IgG-HRP (Biolegend)] diluted 2000x in block buffer were added per well followed by 1-hour incubation at room temperature. 100µl/well TMB reagent (Thermo) was added followed by 10-minute room temperature incubation in the dark. The reaction was stopped by adding 50µl 2M sulfuric acid to each well. The optical density at 450 nm (OD450) was measured on a microplate reader. Each serum dilution was tested in triplicate.

2.6 Evaluate cellular immune response by restimulated splenocytes

Spleens were removed from mice and maintained in RPMIl medium containing 10 mM HEPES supplemented with 2 mM glutamine, 1 mM pyruvate, 0.05 mM 2-mercaptoethanol, and 10% fetal bovine serum (FBS). Spleens were gently ground through a 70µm cell strainer in 10ml medium to generate a single-cell suspension of splenocytes. After centrifugation at 1500 rpm for 5 minutes, resuspended cells in 3 mL ACK lysis buffer to remove erythrocytes. The remaining cells were washed, counted and resuspended in culture medium. Cells were seeded in 96-well U bottom plates at 1,000,000 cells/well in 200 µL media. Cells were stimulated with 5 µg/mL OVA, Concanavalin A (ConA,positive control) (Sigma), or complete medium (negative control). After 48 hours culture, supernatant was collected from wells and centrifuged to remove cells in the suspension. IFN-γ and IL-4 (Peprotech) secreted by restimulated splenocytes were measured following manufactures''

instruction to determine cellular response. All samples were prepared with positive and negative controls and were tested in triplicate.

3. Results

3.1 Cell infiltration and tissue response

Cell recruitment was observed as early as 24 hrs at the scaffold periphery and by 48 hrs throughout the scaffolds. Cells in 40-µm scaffolds were evenly distributed and there was no cell accumulation on the scaffold edges (**Figure 4.2, B, E**). Cells apparently have full access to the entire scaffold interior and potentially any vaccine vector being released from within the scaffold, as well as an easy exit route to the LN upon antigen uptake. On 20-µm scaffolds, cell accumulation occurred as early as 3 days, which prevented more cells from entering the scaffold. After 7 days, fewer cells were observed within the 20-µm scaffolds than 40- and 90-µm scaffolds (**Figure 4.2, A, H**). Cells were distributed throughout 40- and 90-µm scaffolds after 3 days. However, as the 90-µm pore size allowed for multiple cells in each pore, we observed cell clusters lining the pores and forming fibrous capsules on the surface over time (**Figure 4.2, C**), potentially hindering egress to LN. Cell adhesion and fibrous structures were observed on all PDMS scaffolds including the 40-µm PDMS scaffolds (**Figure 4.2, D**).

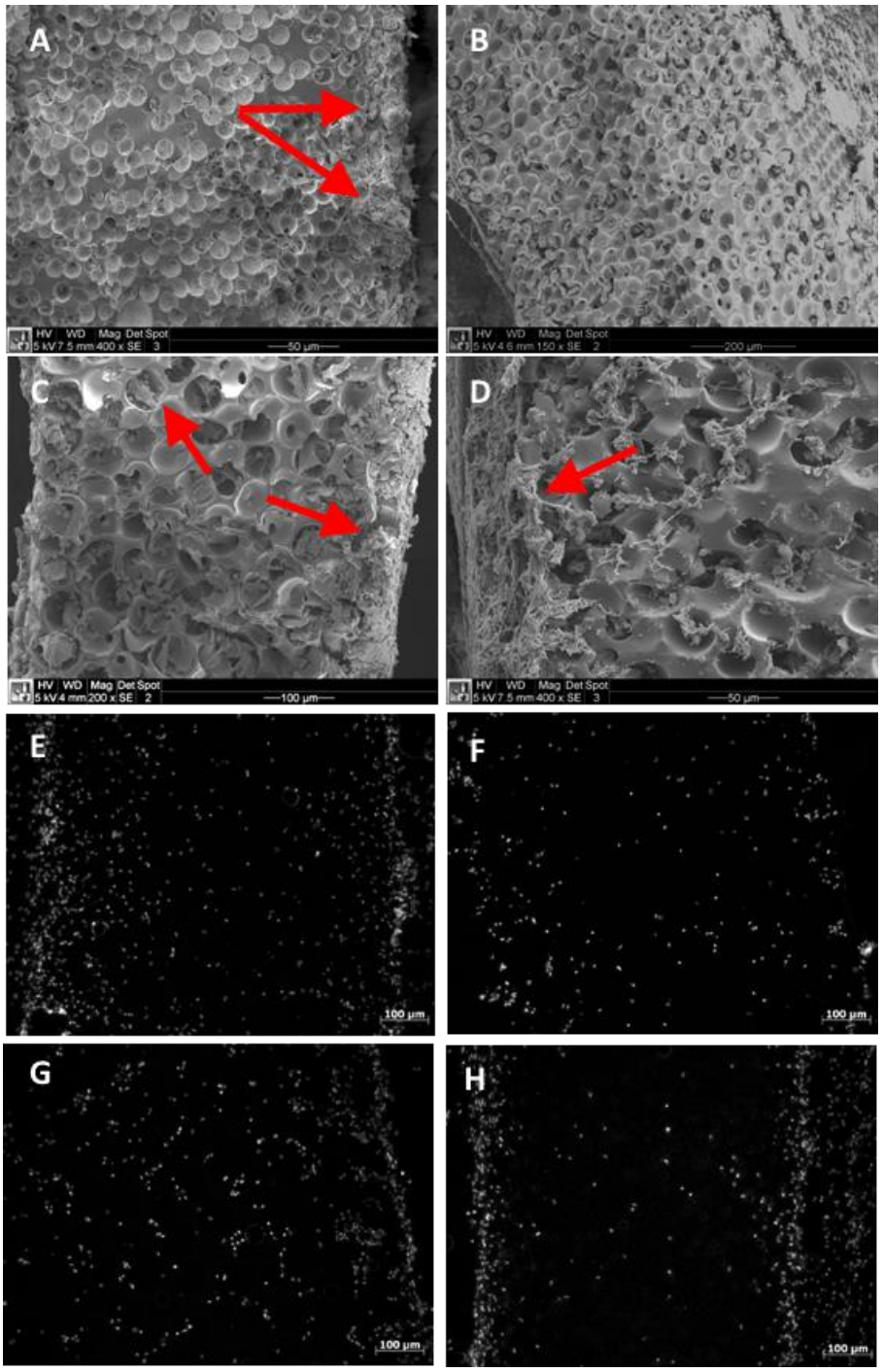

Figure 4.2 *In situ* cell infiltration analysis. SEM analysis of samples after 3 or 7 days' implantation of (**A**) 20-µm HEMA scaffold, Day 3; (**B**) 40-µm HEMA scaffold, Day 7; (**C**) 90µm HEMA scaffold, Day 3; (**D**) 40-µm PDMS scaffold, Day 7. Fluorescence imaging of DAPI stained cells within pHEMA scaffolds after 3 or 7 days' implantation; (**E)** 40-µm HEMA scaffold, Day3, (**F)** 90-µm HEMA scaffold, (**G**) 90-µm HEMA scaffold, Day7, (**H**) 20-µm HEMA scaffold, Day7.

3.2 APC phenotype at implantation site

To further understand the immune cell population at the implantation site, cells were extracted from the scaffolds and were analyzed by flow cytometry. As shown in **Figure 4.3**, similar levels of CD11c+ DC subpopulation (~6%) were observed at all scaffolds after 3 days' implantation (**Figure 4.3, A**). DCs number decreased by day 7 with smaller pore sizes (20, 40 μm) retaining more DCs than bigger pore sizes (90 μm). (**Figure 4.3**, **B**). A majority of the DCs (>60%) showed early signs of maturation by expressing MHCII molecules (**Figure 4.3, E, F**) and this did not change over the course of one week. While there was not a significant difference between DCs activation levels at early time points, both HEMA and PDMS scaffolds of 20μm pores contained a considerable amount of activated DCs at Day7 (**Figure 4.3, H**). Macrophage population reduced from 11.5-13.2% on day 3 to 5.5-8.4% on day 7 with no obvious trend observed based on pore size or material.

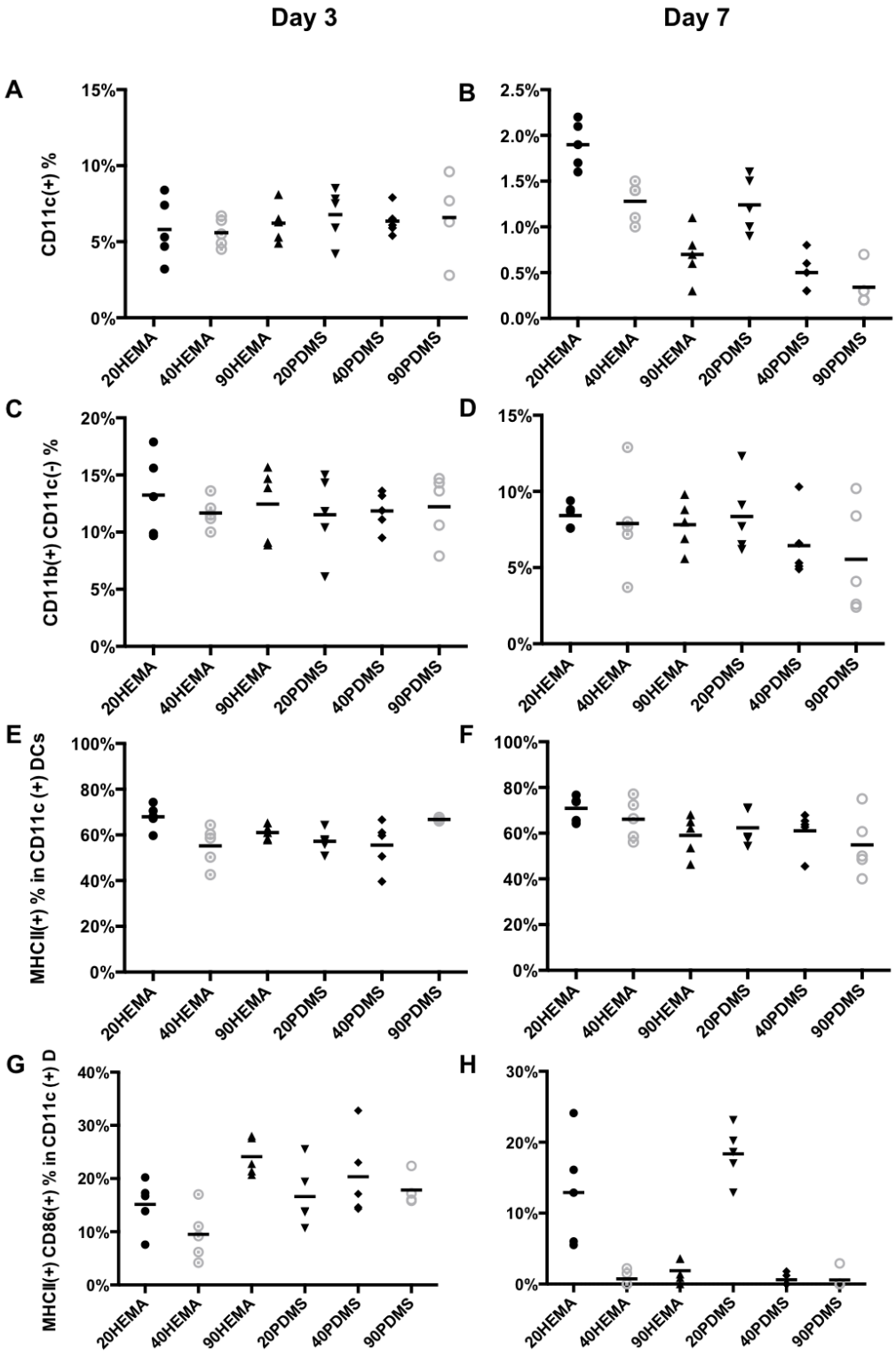

Figure 4.3 Surface marker expression of cells extracted from scaffolds. (**A**), (**B**) CD11c(+) CD11b (-) DCs; (**C**) (**D**) CD11b(+) CD11c(-) macrophages; (**E**), (**F**) MHCII (+) DCs; (**G**), (**H**) MHCII(+) CD86(+) mDCs. (**A**), (**C**), (**E**), (**G**) = Day 3; (**B**), (**D**), (**F**), (**H**) = Day7.

3.3 Scaffold adjuvant effect evaluated with co-delivered OVA

3.3.1 Histological analysis

After 3 weeks, all scaffolds showed some levels of cell infiltration and vascularization (**Figure 4.4**). This was considered beneficial for tissue integration, cell recruitment and drug delivery. pHEMA scaffolds demonstrated better vascularization than PDMS scaffolds in each treatment condition. After incorporating the OVA antigen, the fibrous layer was thicker in both materials (**Figure 4.4 A and B, D and E**). This was expected since host response occurs at implantation site and immunogenic entities induce stronger acute immune response. However, it may become a concern if the fibrous tissue creates a barrier for drug delivery. pHEMA scaffolds exhibited better vascularization than PDMS scaffolds after 3 weeks implantation.

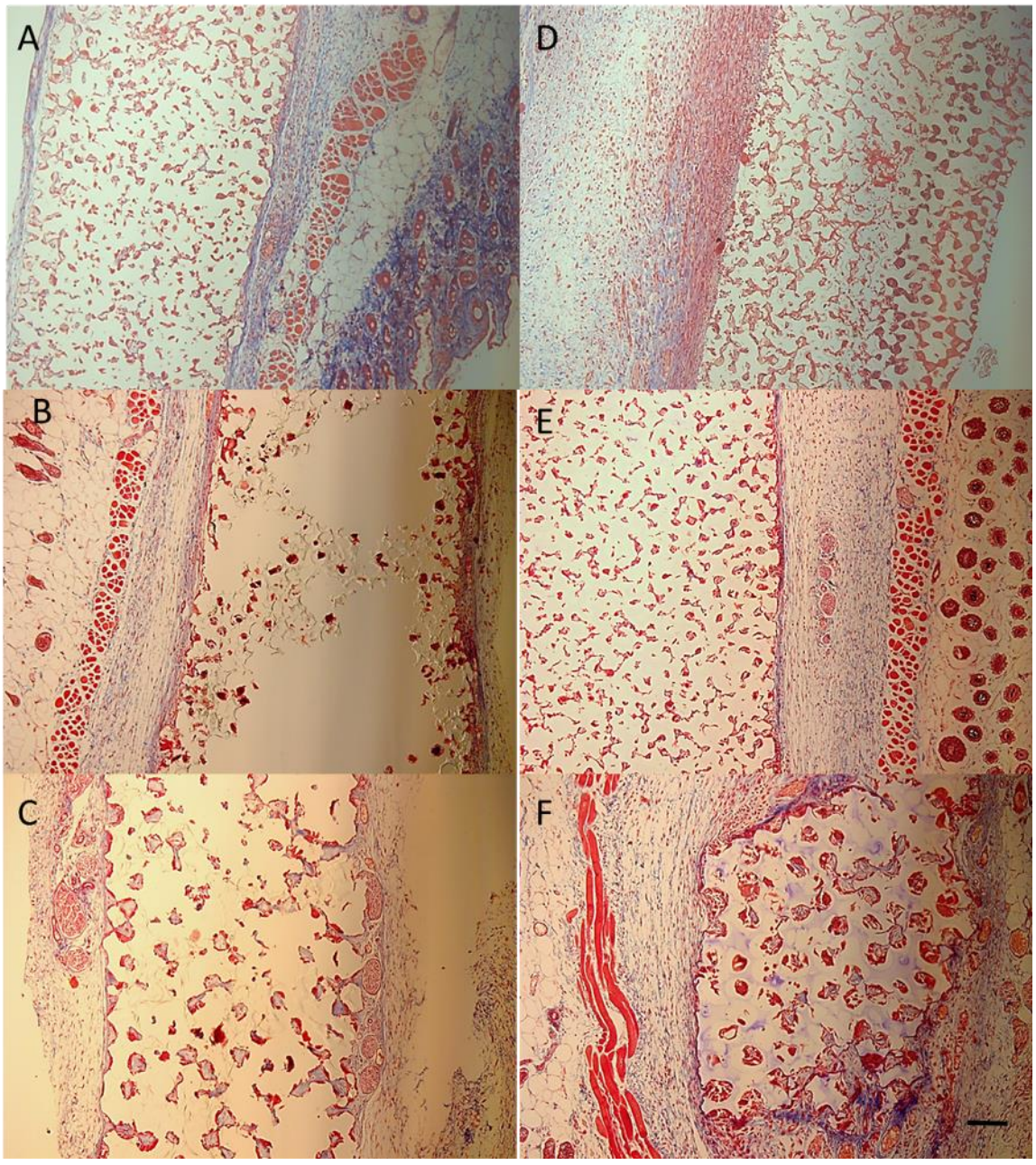

Figure 4.4 Masson's trichrome stain of tissue sample after 3 weeks implantation. Scaffolds shown above are (**A**) 40µm PDMS; (**B**) 40µm PDMS immunized with OVA; (**C**) 90µm PDMS immunized with OVA; (**D**) 40µm pHEMA; (**E**) 40µm pHEMA immunized with OVA; (**F**) 90µm pHEMA immunized with OVA. Scale bar = 100 µm.

3.3.2 Humoral and cellular response

Blood samples were collected each week and anti-OVA specific IgG level was measured by ELISA at the end of the study (**Figure 4.5**). Biomaterials alone induced base level immune responses similar to PBS. This confirmed that these two materials were not immunogenic. Among all the biomaterial scaffolds, only 40μm PDMS was able to promote slightly higher but not significant anti-OVA IgG production. Compared to the OVA alone group, biomaterial groups were able to induce higher antibody production during the first and second week, which could arise from the tissue damage associated with surgery and subsequent acute inflammation. No significant difference in immune response was seen with pore size. Overall, the adjuvant effect from biomaterial scaffolds was not as significant as we expected. One possible explanation for this was that OVA solution was injected at implants location instead of embedded within scaffolds. Without any additional adjuvant, the antigen only had transient exposure to the cells.

To measure cellular response, splenocytes were isolated and restimulated with OVA, ConA and complete medium. IFN-γ and IL-4 secreted by splenocytes were measured by ELISA as an indication of T cell response. Only ConA-stimulated splenocytes had expressed elevated levels of IFN-γ. OVA-stimulated splenocytes had similar IFN-γ level as control (**Figure 4.6**). All groups including positive controls produced base level IL-4 after stimulation. This was consistent with other measures indicating a Th1 skewed immune response (X.-Y. Zhang, Liu, Wang, Wang, & Gao, 2003). Other groups have reported that C578L/6J mice do not produce IL-4 upon stimulation (Huang, Ostroff, Lee, Specht, & Levitz, 2010). A restimulation protocol with different antigen dosage and stimulation time was tested and no significant results were observed (data not shown).

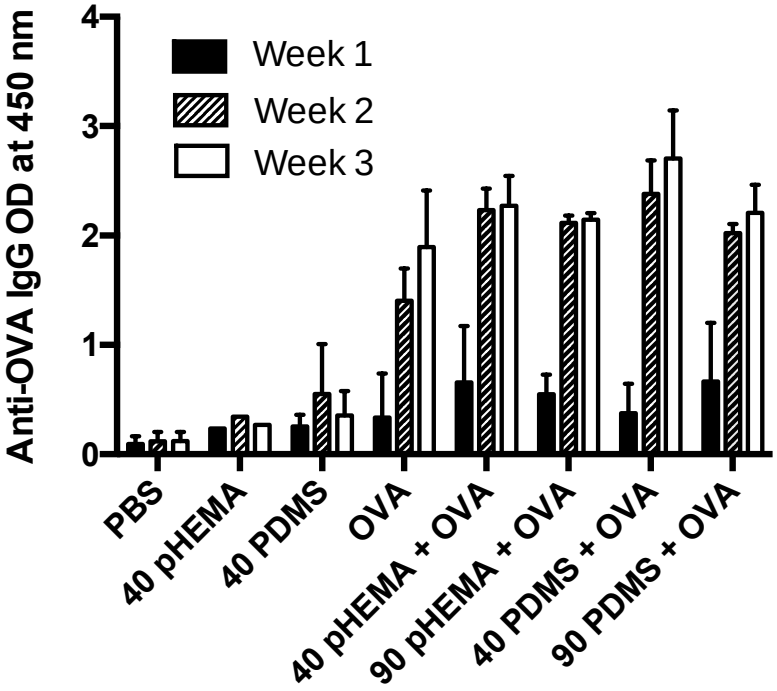

Figure 4.5 Concentration of serum anti-OVA IgG over the course of 3 weeks. Data was represented in mean standard ± deviation.

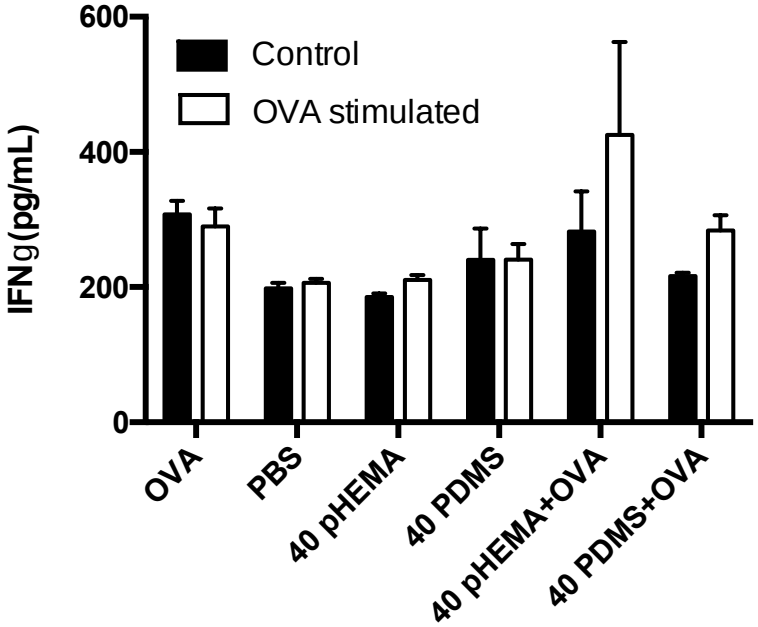

Figure 4.6 Concentration of IFN-γ secretion by splenocytes restimulated by OVA or medium for 24 hours. Data was represented in mean standard ± deviation.

4. Discussion

When implanted in C57BL/6J female mice, immune cells (both CD11b and CD11c positive APCs) were found around scaffolds two days after implantation. As more cells migrated to the implantation site, we observed different infiltration patterns based on the material and pore size. In terms of pore size, both 20 μm and 90 μm pores hindered overall cell infiltration to some degree. When cells migrated to the 20μm scaffolds, cell accumulation occurred as early as 3 days and it prevented future cell infiltration. In contrast, 90 μm pores allowed for abundant cell infiltration initially. However, each 90-μm pore in the scaffold contained multiple cells that eventually lead to the formation of cell clusters and fibrous structures. This also explains the highest level of DC prematuration observed in 90um pHEMA scaffolds *in vivo*, which we did not expect based on the *in vitro* results. In a previous study (Iribarren et al., 2002), injectable PDMS led to a prolonged recruitment of immune cells and enhanced APC activity. Even though a more hydrophobic material (PDMS) can potentially induce higher levels of DCs activation that is ideal for an adjuvant, it is also expected to accumulate more protein on the surface and have a stronger foreign body reaction, which is not suitable to be used as a scaffold-based vaccine delivery platform. This poses the questions of (a) whether immune cells will have full access to a vaccine vector being released from within the scaffold, and (b) whether differentiated APCs can successfully navigate the fibrous structure, then leave the scaffold, and migrate to lymph nodes (LNs). In this study, the PDMS scaffold led to a more prominent fibrous structure around the scaffold while pHEMA scaffolds consistently promoted better tissue integration. Among all the scaffolds, 40um pHEMA scaffold demonstrated the best tissue integration, showing no fibrous structure and almost no cell accumulation on the edges.

Although all scaffolds to some degree demonstrated the capacity to promote DC recruitment, and subsequent retention and activation at the implant site, no adjuvant effect was observed when OVA protein antigen was co-delivered.

5. Conclusion

When implanted subcutaneously, activated DCs were observed at the implantation site for up to a week. Smaller pore sizes were found to be more favorable for CD11c+ DCs accumulation and activation. Additionally, a uniform cell distribution was observed in scaffolds with 40 µm and 90 µm pores, indicating a minimum pore and throat size was necessary to guarantee sufficient cell infiltration.

Having demonstrated the scaffolds' ability to recruit immune cells and maintain them at the implantation site, the adjuvant effect of pHEMA and PDMS scaffolds with 40 and 90 µm pores was assessed with a model antigen, OVA. While OVA combined with scaffolds did promote faster antigen specific antibody production in the first two weeks, overall adjuvant effect was not significant and no cellular response was observed.

Overall, these results combined with the *in vitro* findings support the hypothesis that changing the pore and throat sizes of a scaffold could enhance cell maturation and cell accumulation at the implantation site. Additional adjuvants can be incorporated into the scaffold design to enhance the adjuvant effects to co-delivered vaccines.

Chapter 5 *In vitro* evaluation of polymer and lipid based carriers for mRNA delivery

1. Introduction

Multiple studies have reported that naked single stranded mRNA (ss-mRNA) has a poor ability to transfect cells and has a very short half-life *in vivo* (Phua et al., 2013). The enzymatic degradation potential poses a great barrier for the development of single stranded mRNA therapeutics applications. Numerous strategies have been developed to condense anionic nucleic acids with various cationic lipids and polymers; mostly for plasmid DNA. Condensing nucleic acids with cationic molecules helps stabilize the nucleic acids while facilitating the endosomal escape process. While Poly (ethylenimine) (PEI) has been considered one of the most efficient polymers for gene delivery(Godbey et al., 1999), lipid based carriers have shown better capacity at facilitating mRNA transfection (Yamamoto et al., 2008). It is hypothesized that lipids and polymers with smaller molecular weights have a weaker bonding strength to mRNA than larger polymer molecules, thus helping to facilitate the release of mRNA in cytoplasm, which is necessary for ribosome recognition and translation (Bettinger et al., 2001; Rejman et al., 2010). Many systems such as lipoplexes and lipid nanoparticles have incorporated both lipid and polymer components to optimize both transfection ability as well reduce cytotoxicity (Persano et al., 2017; Su et al., 2011).

Concomitantly, there has been ongoing efforts to optimize the structure of mRNA for better stability and transfection efficiency. One approach is to utilize self-replicating mRNA (sr-mRNA) that is a viral replicon derived from viruses (Geall et al., 2012; Schlesinger, 2001). An RNA replicon contains only non-structural viral genes so the vector retains the ability to amplify the

gene of interest without the viral toxicity components. The self-replicating nature of sr-mRNA increases mRNA templates and therefore will enhance antigen provision compared to protein-based and non-replicating nucleic acid vaccines.

In this section, multiple lipids (Lipofectamine™ MessengerMAX™, Stemfect™) and polymers (*in vivo*-jetPEI, PBAE) were evaluated as mRNA gene carriers. Upon forming polyplexes or lipoplexes with mRNA, the resultant polyplex particle size was measured with DLS. The cytotoxicity potential and transfection ability of the polymer/lipid: RNA complexes were evaluated in a range of cell lines, including dendritic cells. Transfection with both regular ss-mRNA and Sindbis virus based sr-mRNA were compared *in vitro* to explore the potential of using sr-mRNA to improve delivery efficiency and expression duration. Other factors that determine mRNA's efficient expression *in vivo* includes delivery route, formulation, etc;, which will be discussed in detail in the next chapter.

2. Experimental methods

2.1 Plasmids and in vitro transcription of mRNA

Plasmid DNA was prepared using the QIAprep Spin Miniprep Kit (Qiagen). Plasmid pGEM4Z-GFP-A64 (a gift from E. Gilboa, University of Miami) encoding eGFP with a synthetic poly-A tail has been previously described(Boczkowski, Nair, Nam, Lyerly, & Gilboa, 2000). Plasmid SinRep-GFP (a gift from S. Schlesinger, Washington University School of Medicine) encoding eGFP with a synthetic poly-A tail has been previously described(Agapov et al., 1998). pGEM4Z-GFP-A64 was linearized by SpeI. Linear DNA was purified using a GeneJET Gel Extraction and DNA Cleanup kit (Thermo Scientific), and used as templates for *in vitro* transcription using a

mMESSAGE mMACHINE SP6 Kit (Ambion). SinRep-GFP was linearized by XhoI. Linear DNA was purified and used as templates for *in vitro* transcription using a mMESSAGE mMACHINET7 kit. The resultant mRNA was purified using a RNeasy MinElute Cleanup Kit (Qiagen).

2.2 Synthesis of poly (β-amino ester) (PBAE) gene carrier

Acrylate-terminated poly (β-amino ester) was synthesized by mixing 1, 4-butanediol diacrylate (3.532g, 17.8 mmol) with 5-amino-1-pentanol (1.533g, 14.8 mmol) for 24 h at 90 ^{O}C in the dark. End-chain-capping reactions were performed by adding 9.1 g of tetrahydrofuran (THF) to 5 g of acrylate-terminated poly (β-amino ester), vortexing, and then transferring to a 100mL flask with a stir bar. 40mL of 0.25 M end-capping amine solution was then added and the mixture was left stirring at room temperature in the dark for 24 h. The resultant polymer was purified in the diethylether twice and dried in the vacuum oven.

2.3 Nuclear magnetic resonance (NMR) spectroscopy

The ^{1}H-NMR spectra of all dried PBAE and final lyophilized polymers were acquired using a Bruker AV 500 at 10-20 mg/mL polymer in DMSO. The monomer compositions of PBAE were determined by the integration of the peaks described in **Figure 5.1**.

2.4 Formulation of mRNA-polymer polyplexes and lipoplexes

PBAE polyplexes were formed by combining equal volumes of mRNA (0.02 μg/μL) and PBAE solution (0.18 μg/μL) in sodium acetate solution for 15 min at room temperature. *In vivo*-jetPEI polyplexes were formed by diluting mRNA and *in vivo*-jetPEI to 0.12:1 v/w PEI:mRNA ratio in

equal amount of 5% glucose solution and mixing for 15 min at room temperature. The resultant N/P ratio for PBAE and *in vivo*-jetPEI polyplexes are 10 and 6, respectively. Lipoplexes were formed by combining mRNA and liposome at a 4:1 v/w Stemfect™: mRNA and 1.5:1 v/w Lipofectamine™ MessengerMax™ (LF-MM):mRNA ratio in Stemfect™ buffer and reduced serum Opti-MEM™ respectively in accordance with the manufacturer's protocols. The total formulation volume for all polyplexes and lipoplexes in this study were 100 μl per 1 μg mRNA.

2.5 Polyplexes size and distribution

The sizes of the polymer/mRNA polyplexes and liposome/mRNA lipoplexes were determined by DLS measurements using a Malvern Zetasizer Nano ZS. Polyplexes and lipoplexes were analyzed at a mRNA concentration of 10 μg/mL and the mean diameters are reported as the Z-average ± standard deviation.

2.6 Cell culture

All cell culture medium and reagents were obtained from Gibco unless otherwise specified. The BHK-21 hamster fibroblast cell line (ATCC) was maintained in Eagle's Medium supplemented with 10% FBS and 1% penicillin-streptomycine.

The DC2.4 murine dendritic cell line (a gift from K.L. Rock, University of Massachusetts Medical School) was maintained in RPMI 1640 containing L-glutamine supplemented with 10 mM HEPES, 0.1 mM non-essential amino acids, 55 μM 2-mercaptoethanol, 10% FBS, and 1% penicillin-streptomycin.

The JAWsII murine dendritic cell line (ATCC) was maintained in alpha minimum essential medium supplemented with 1.5g/L sodium bicarbonate, 2 mM L-glutamine, 5ng/mL GM-CSF, 20% FBS, and 1% penicillin-streptomycin.

Murine bone marrow-derived dendritic cells (BMDCs) were obtained and isolated from the femurs and tibiae of 6-8 week-old female C57BL/6 mice. Cells were cultured in Petri dishes in 10 mL complete medium containing 20 ng/mL granulocyte macrophage colony-stimulating factor (GM-CSF, Peprotech, Rocky Hill, NJ). 10 mL fresh medium containing 20 ng/mL GM-CSF was added on Day 3, and medium was changed on Day5. Cells were harvested and used for experiments on Day 7.

2.7 mRNA in vitro transfection

Polyplexes and lipoplexes were formulated as described above using ss-mRNA-GFP and sr-mRNA-GFP, and added to the cells at 1 μg mRNA/well. Cell medium was added to each well to obtain a total volume of 1 mL/well and the poly/lipoplexes were allowed to incubate with cells for 24 or 48 h. After this time, the cells were washed and collected by PBS-based cell dissociation buffer (Invitrogen) or 0.25% trypsin-EDTA, and resuspended in DPBS containing 2% FBS and 0.2 μg/mL propidium iodide (Invitrogen). To determine cell viability and GFP expression levels, 10,000 events per sample gated on single cells were acquired on a BD LSRII flow cytometer (BD Biosciences) and analyzed using FlowJo software. In some experiments, cells were washed once with DPBS and then fixed with 4% paraformaldehyde (PFA) for 15 min, then imaged on a Zeiss Axio Observer Z1 fluorescence microscope with an ApoTome optical sectioning attachment.

3. Results

3.1 PBAE polymer synthesis and characterization

PBAE polymer was synthesized as shown in **Scheme 5.1**. Proton nuclear magnetic resonance (1H NMR) spectral analysis on samples of the synthesized poly (β-amino ester) gene vector (**Figure 5.1**) were performed to confirm that the resulting material had the desired chemical structure.

NMR analysis confirmed that the synthesized polymers exhibited all expected resonances and were free of residual monomers. No acrylate signal was detected in the range of 6-7 ppm, proving the end-capping step was successful.

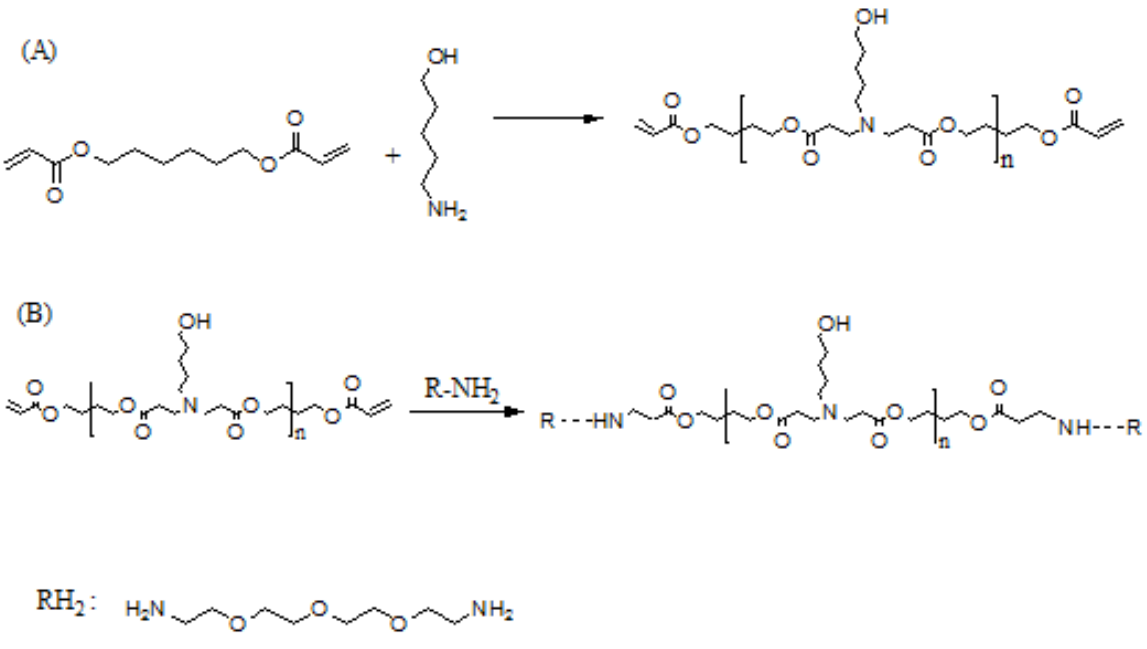

Scheme 5.1 Synthesis of PBAE polymers.

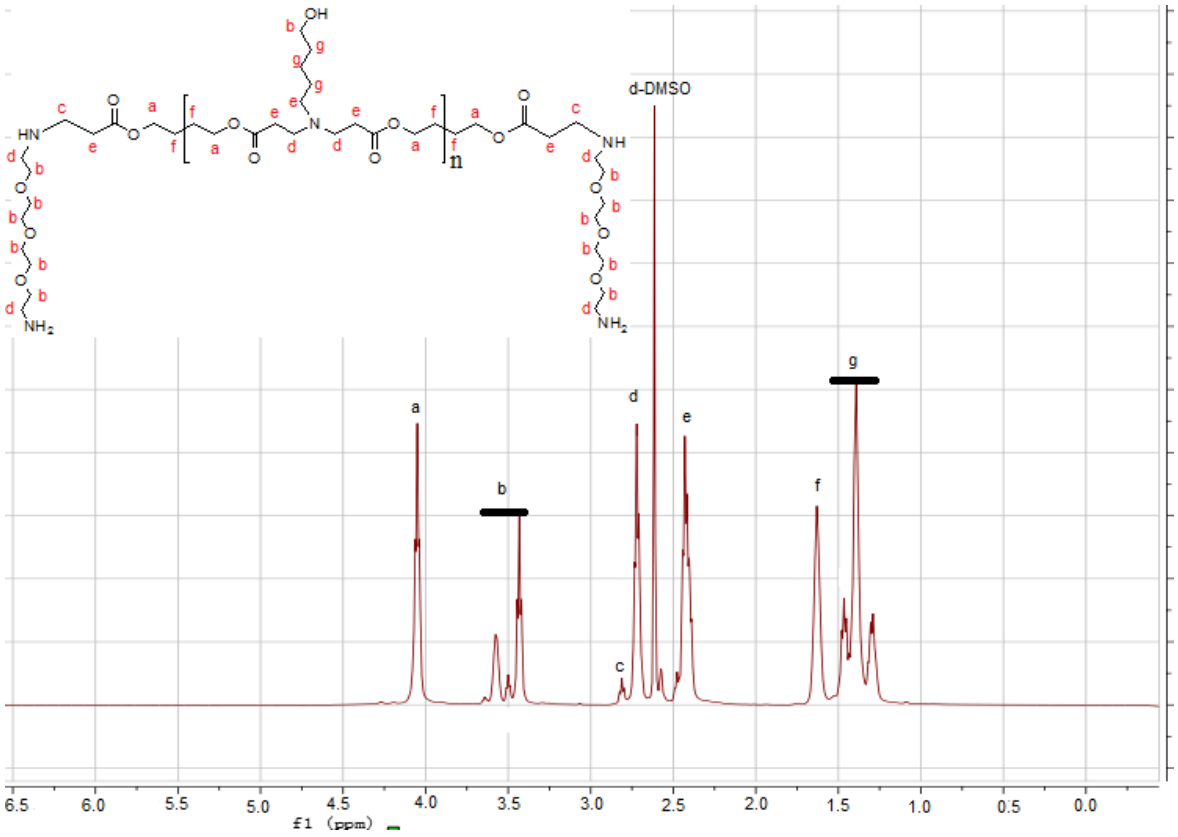

Figure 5.1 H1 NMR spectrum (500 MHz, d-DMSO) of poly (b-amino ester) gene vector. Monomer compositions were determined by integration of peaks (a-g) shown on top left.

3.2 Size distribution and zeta potential of polyplexes and lipoplexes

Polyplexes and lipoplexes were characterized by DLS for particle size and zeta potential analysis (**Table 5.1**). Except for LF-MM lipoplexes, other particles were monodispersed and under 200 nm.

Table 5.1 DLS measurements of poly/lipoplexes sizes

Poly/lipo-plexes	Size (nm)
In vivo-jetPEI	143 ± 43
PBAE e6	184 ± 19
LF-MM	552 ± 215
Stemfect	138 ± 18

Diameters are calculated from z-average size ± standard deviation calculated from the PDI.

3.3 In vitro transfection of pGEM-GFP with various compounds

The ability of the polymers and liposomes to mediate mRNA transfection *in vitro* was evaluated in baby hamster kidney fibroblast cell lines, BHK-21; murine dendritic cell lines, DC2.4 and JAWsII; and murine primary bone marrow derived dendritic cells (BMDC). While all reagents exhibited comparable abilities in transfecting BHK fibroblast cells, most of them were not efficient at facilitating mRNA transfection in dendritic cells. Twenty-four hours after vector exposure, transfection rate was lower than 10% and 3% for dendritic cell lines and primary cells, respectively. In contrast, transfection efficiency with Stemfect™ lipoplexes in the same DC cell type were from 3 to 6 times higher than the rest reagents tested. Also, Stemfect™ lipoplexes were more efficient in transfecting DC2.4 cell lines (53.3% GFP+) than JAWsII cell lines (30.4% GFP+) (**Figure 5.3**).

Cytotoxicity of the polymer or lipid carriers was also evaluated. While cells transfected with commercial standard LF-MM had 70~80% viability after 24 h, over 90% cells transfected with Stemfect™ were still viable 24 h later, which is very close to the control group that contained no RNA. In contrast, although PBAE demonstrated similar transfecting capability as LF-MM, it appeared to be more toxic to the cells tested, especially to JAWsII cells. Only 20% cells were still viable after co-culture for one day. In more robust BHK cell lines, such cytotoxicity effects are reflected in morphological changes. Cells transfected with Stemfect™ lipoplex showed the typical elongated morphology for BHK cells. Parallel cultures of BHK, 24 h after exposure to *in vivo* jet-PEI and PBAE polyplexes, produced cells with more rounded shapes along with cell clumps. Such morphological changes were accompanied by slower growth or cell death as evidenced in lower cell density (**Figure 5.2**)

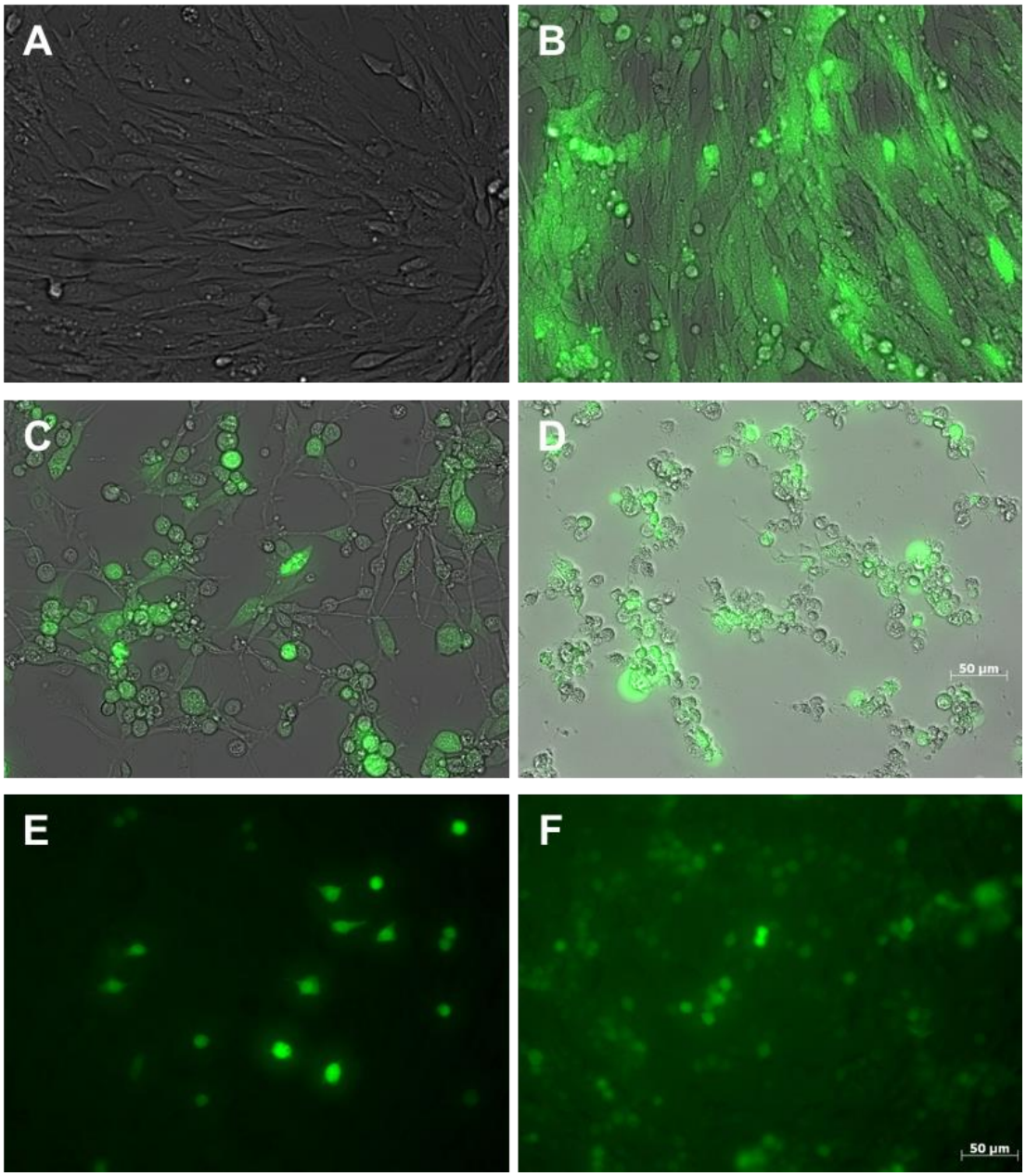

Figure 5.2 Cell morphology and GFP expression upon transfection with mRNA poly/lipo-plexes. BHK fibroblast cells upon transfection with (**A**) control with no mRNA; (**B**) Stemfect™/GFP; (**C**)*in vivo*-jetPEI/GFP, (**D**) PBAE/GFP. JAWsII cells transfected with (**E**) LF-MM/GFP; (**F**) Stemfect™/GFP. Scale bar is 50 µm.

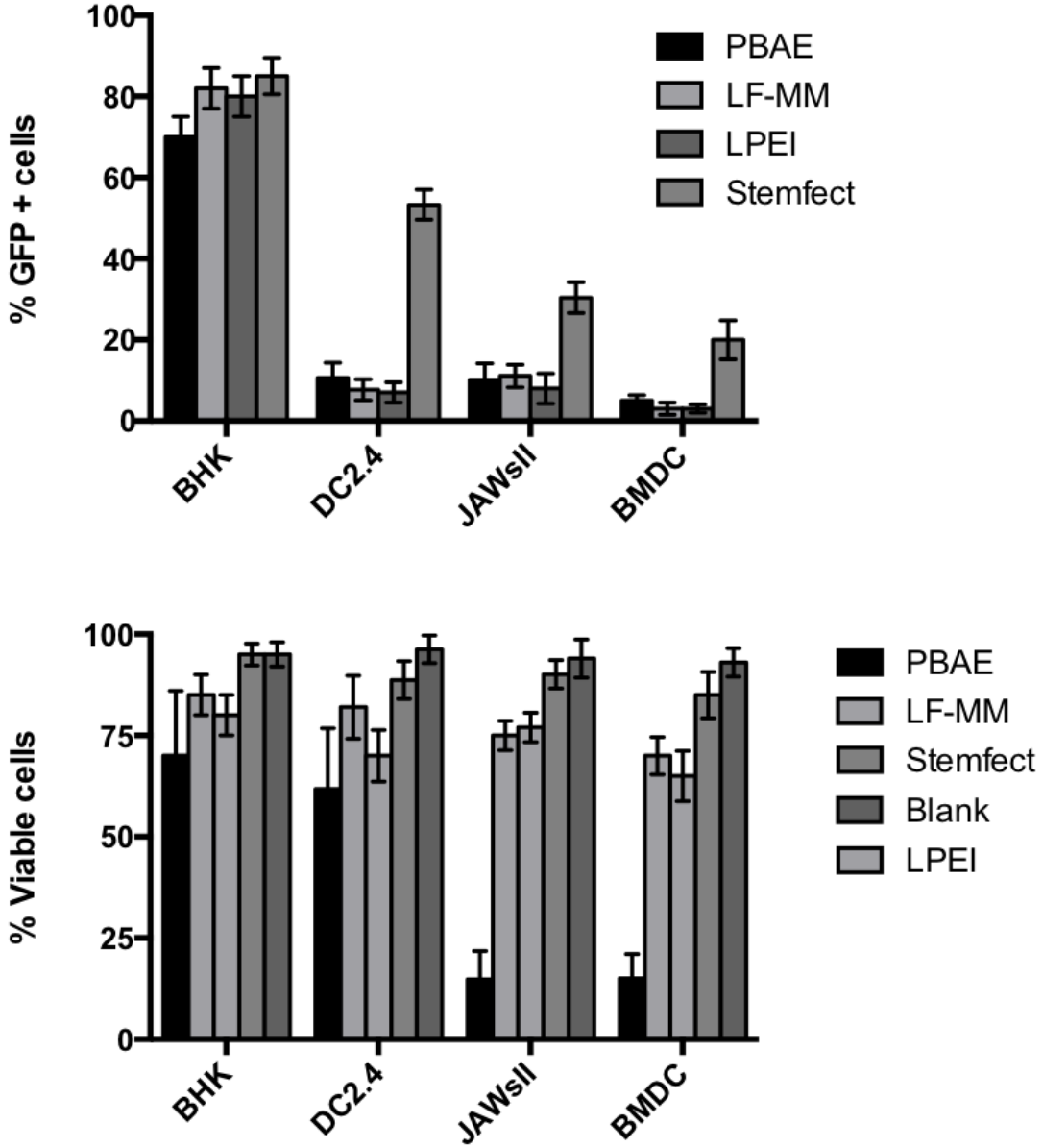

Figure 5.3 Transfection efficiency (**B**) Cell viability after 24 h transfection with poly/lipo-plexes. Data are from a single representative experiment conducted in triplicate ± standard deviation.

3.4 In vitro transfection of sr-mRNA

The potential of using sr-mRNA to improve transfecting efficiency was evaluated. In a 12 h time course, ss-mRNA-GFP vectors were expressed faster than sr-mRNA-GFP in the initial 5 hours. However, by 12 h 92.4% BHK cells were expressing SR-RNA-GFP in comparison to 71.9% transfected with ss-mRNA-GFP (**Figure 5.4, A**). However, same pattern was not observed in dendritic cell lines or BMDC. Almost no GFP signal was detected in dendritic cells transfected with sr-mRNA-GFP poly/lipo-plexes. It was noted that sr-mRNA induced more morphological changes and higher cell mortality after 48 h compared to regular mRNA (**Figure 5.4, B, C**).

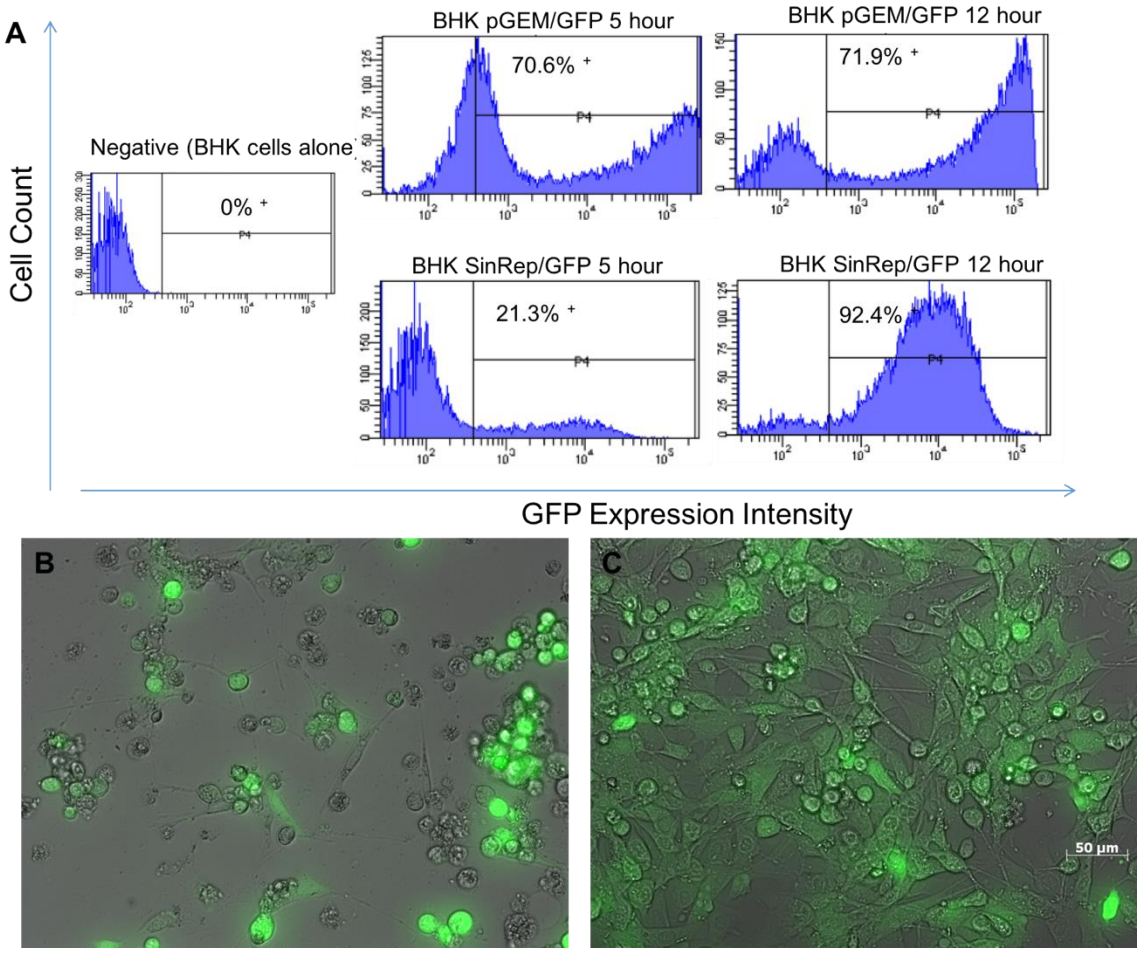

Figure 5.4 Transfection with sr-mRNA-GFP. BHK cells transfected with ss-mRNA-GFP or sr-mRNA-GFP complexed with *in vivo*-jetPEI (**A**) Comparason of transfection efficiency at 5h vs. 12h; BHK cell morphology and expression after transfection with (**B**) sr-mRNA-GFP; (**C**) ss-mRNA-GFP.

4. Discussion

Lipofectamine and jetPEI are the most commonly used commercially available lipid-based and polymer-based carriers, respectively and are usually used as positive controls to evaluate alternative carriers. Other carriers in these two categories, PBAE and Stemfect^{TM}, were selected to compare against lipofectamine and jetPEI.

In general, it was observed that lipid based LF-MM and Stemfect^{TM} carriers are more effective than polymer based *in vivo*-jetPEI and PBAE at mediating mRNA expression *in vitro*, which is consistent with most current studies in mRNA delivery. It has been reported by some groups (Bettinger et al., 2001; Rejman et al., 2010) that release of mRNA from a carrier in the cytoplasm is necessary for ribosomal recognition. Therefore, the binding strength between mRNA and the cationic polymer or lipid will greatly affect mRNA expression efficiency. Bettinger *et al*. demonstrated that single stranded mRNA binding to cationic polymers is stronger than pDNA binding. Polymers with larger molecular weight have higher affinity to mRNA than polymers with smaller molecular weight. This explains why polymers such as PEI (22 kDa, 25 kDa) and poly(L-lysine), which are preferred for DNA delivery due to their great stability, led to poor results for mRNA delivery.

The Stemfect^{TM}/mRNA transfection efficiency in dendritic cells was compared in a similar study conducted by Phua *et al.* (Phua et al., 2013). While Stemfect^{TM}/mRNA has a varied ability to mediate mRNA expression in different dendritic cell lines (DC2.4 > JAWsII > BMDC), its overall reported transfection rate is notably higher than other carriers. Over 60% BMDC were expressing GFP protein 8 h post-culture with the complex (Phua et al., 2013). A modified method of preparing lipoplexes with sodium acetate buffer (pH=5) with 5% glucose was reported in the Phua study,

which produced smaller particle sizes. But it is unclear whether this factor contributed to the higher transfection efficiency.

PBAE: ss-mRNA polyplexes showed comparable transfecting ability to the commercially available lipofectamine and Stemfect^{TM}. However, PBAE also exhibited higher cytotoxicity to cells, which is commonly seen with cationic polymers. PEG and various lipids have been used to shield the charge on the surface of cationic polymers and thus to reduce cytotoxicity (Uchida et al., 2012).

In this section, the potential of using sindbis virus based self-amplifying replicon RNA was also explored. Alphaviruses are generally cytopathic. Upon infection of alphavirus replicons, cell protein synthesis is inhibited and cells die after 24 – 36 h (Schlesinger, 2001). This is consistent with what we have observed in the study. Different non-cytopathic mutants of Sindbis virus have been developed (Dryga, Dryga, & Schlesinger, 1997; Perri et al., 2000) . Enhanced expression and cell viability were demonstrated only in cells that do not induce interferons (BHK, CHO and Vero). This may explain the lack of GFP expression and high cell mortality in DCs. So while there have been reported studies of successful induction of immune response from alphavirus based sr-mRNA (Geall et al., 2012), their use in DC immunization has not been reported.

On the other hand, non-cytopathogenic self-amplifying mRNA such as pestivirus and flavivirus offered advantages for prolonged antigen maintenance and may be more suitable than alphavirus-based sr-mRNA for transfecting slow dividing antigen presenting cells (Rodríguez-Gascón, del Pozo-Rodríguez, & Solinís, 2014). Demoulins *et al*. successfully delivered RepRNA derived from the pestivirus classical swine fever virus (CSFV) to DCs with PEI based polymers (Démoulins et al., 2016). Non-cytopathic sr-mRNA is considered to be a more suitable alternative for gene delivery to DCs and is worth further investigation.

5. Conclusion

A series of commercial and synthesized polymer and liposomes; *in vivo*-jetPEI, LF-MM, PBAE, and Stemfect™ were evaluated for their ability to facilitate intracellular ss-mRNA and sr-mRNA delivery. All complexes had mono-distributed polyplex particle size that were under 200nm except for LF-MM. While sr-mRNA enhanced transfection rate and expression duration in BHK cells compared to ss-mRNA, sr-mRNA appeared to be pathogenic and was not suitable to transfect slow dividing dendritic cells, regardless of transfecting agents used. Among complexes tested, Stemfect™ demonstrated superior capacity in facilitating intracellular mRNA delivery across a variety of cell lines, especially dendritic cells while maintaining excellent cell viability.

Chapter 6 Scaffolds-based mRNA delivery

1. Introduction

mRNA has emerged as a promising candidate for vaccine applications in recent years. Strategies have been developed to overcome its instability *in vivo* while targeting APCs efficiently. Various formulations have been developed to protect mRNA from RNases and facilitate its uptake into cells. Also, different routes and strategies have been developed for the administration of mRNA vaccines (Phua et al., 2013). While systemic delivery of mRNA vaccine has limited success, scaffold-based subcutaneous implants present a novel approach to mRNA delivery. Some advantages of implant delivered vaccines are 1) Heterogeneous populations of immune cells are found in the skin, making it an optimal site for vaccination; 2) Unlike other delivery routes, subcutaneous space contains less proteins and nucleases. Subcutaneous delivery can potentially protect RNA from particle aggregation or enzymatic degradation; 3) Scaffolds can serve as a temporary depot for immune cells to mature. Mooney's group has successfully demonstrated the application of scaffolds for DNA vaccines by targeting local dendritic cells. Recently, Zhang *et al.* also demonstrated the repair of critical-sized calvarial bone defects through two-stage delivery of miRNA from PLGA microspheres immobilized on an nanofibrous scaffold (X. Zhang, Li, Chen, Chen, & Ma, 2016). So far, there has been no study demonstrating mRNA delivery from scaffolds to our knowledge.

In chapter 4 and 5, we concluded that both pHEMA and PDMS scaffolds can induce T_H1 type response from DCs and the level of response correlates with the pore size. In this section, mRNA

lipoplexes formulations were optimized (size and bioactivity) for loading onto scaffolds. pHEMA scaffolds were selected for the *in vivo* study due to better long term tissue integration and vascularization as described in Chapter 4. Two strategies were employed to load mRNA poly/lipoplexes on the surface of pHEMA based scaffolds. To load polymer based mRNA complexes into the scaffolds, pHEMA was functionalized with dopamine methacrylamide (DMA), which enabled covalent bonding between amine groups on the polymer and catechol groups on DM. For lipid based mRNA carriers, a combination of adsorption and lyophilization was used to maximize the loading capacity. The loading efficiency and distribution of mRNA were characterized with RiboGreen® staining of mRNA and fluorescent microscopy, respectively. *In vitro* transfection ability of complexed mRNA loaded scaffolds were tested with DC2.4 cell line. Finally, the mRNA (complexed or free form) loaded scaffolds were implanted in mice and compared against s.c. injected mRNA (complexed or free form) for its distribution, stability as well as transgene expression.

2. Experimental method

2.1 pHEMA functionalization with dopamine methacrylamide (DM)

2.1.1 Synthesis of dopamine methacrylamide (DM)

The reaction mixture was prepared in 200 ml of distilled water by adding 20 g of sodium borate and 8 g of sodium bicarbonate in order to protect dihydroxy benzene moiety. Both sodium borate and sodium bicarbonate were saturated in water and demonstrated some insolubility. The aqueous solution was degassed by bubbling argon through it for 20 minutes. 10 g of 3,4-dihydroxyphenethylamine hydrochloride was then added to this solution. 9.4 ml of methacrylate anhydride solution in 50 ml of tetrahydrofuran (THF) was prepared separately and added dropwise

into the aqueous solution containing 3,4-dihydroxyphenethylamine hydrochloride. The pH of the prepared solution was checked with pH indicator paper. In order to keep the reaction mixture moderately basic (pH 8 or above), 2M NaOH solution was added dropwise. The reaction mixture was stirred for 14 hours at room temperature with bubbling argon. At this time, a white slurry-like solution had formed that was then washed twice with 100 ml of ethyl acetate. The resulting solid in the solution was centrifuged and the supernatant acidified to pH 2 with 6M of HCl solution. The organic layer of the solution was extracted three times from the acidified aqueous solution with 100 ml of ethyl acetate. The extracted clear brown organic layer in the ethyl acetate was dried over MgSO4. The solution volume was reduced to around 50 ml with a rotary evaporator before the precipitation appeared. The resulting solution was added to 500 ml of hexane with vigorous stirring to precipitate a brownish solid and then the formed suspension was refrigerated to maximize crystal formation size. To purify, the resulting light brown solid was dissolved in 40 ml of ethyl acetate and precipitated in 500 ml of hexane. The final solid powder was dried in a vacuum overnight.

2.1.2 p(HEMA-DM) polymerization

pHEMA-DM precursor solution was made according to the composition listed in **Table 6.1**. The reaction mixture was then infiltrated into the glass mold surrounding the template and degassed under vacuum for 30 minutes. pHEMA hydrogel was polymerized under broad-spectrum UV from a high-intensity mercury lamp for 10 minutes by photo initiated free-radical copolymerization (**Scheme 6.1**).

Table 6.1 Composition of HEMA-DM polymer precursor solution.

	Mw(g/mol)	D(g/ml)	Wt(g)	V(mL)	moles	Molar ratio
HEMA	130.14	1.08	4.968	4.6	0.0423	90%
DM	221		0.935			10%
TEGDMA	330.3	1.117	0.268	0.240	0.0008	1.9%
Ethylene Glycol	62.065	1.1155	1.673	1.5		
diH_2O	18	1	2.1	2.1		
Irgacure	228.19		0.020			0.2%

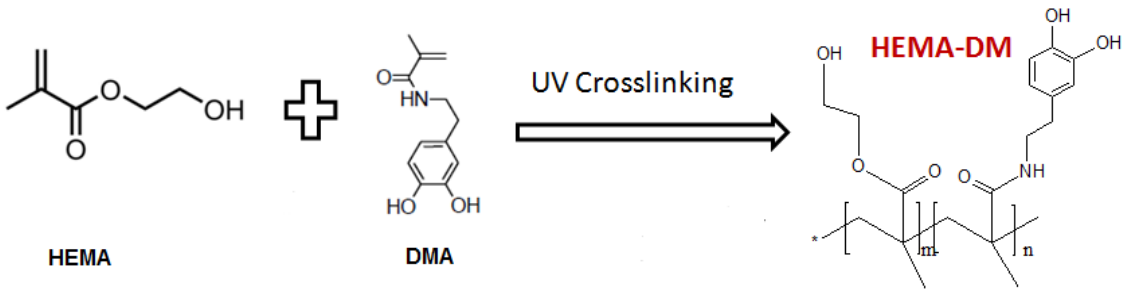

Scheme 6.1 HEMA-DM co-polymerization via UV initiated reaction.

2.2 mRNA polyplexes formulation for coating

2.2.1 Lyophilization effect on size

2 µg ss-mRNA-GFP was formulated into a 200 µl Stemfect^{TM}:mRNA lipoplexes solution as described in Chapter 5 with or without 250 mM trehalose. The solution was flash frozen in liquid nitrogen and then lyophilized. The size of the rehydrated lipoplex was measured with DLS using

a Malvern Zetasizer Nano ZS. Polyplexes and lipoplexes were analyzed at mRNA concentration of 10 μg/mL and the mean diameters are reported as the Z-average ± standard deviation.

2.2.2 In vitro transfection of lyophilized mRNA: Stemfect™ lipoplex

Bioactivity of lyophilized mRNA: Stemfect™ lipoplexes were evaluated with an *in vitro* transfection assay. BHK cells were seeded in 24-well plates at 150,000 cells/well, in 1 mL complete medium and allowed to adhere overnight. 200 μL lipoplexes solution containing 1 μg ss-mRNA was added in each well. After 24 h, cells were collected by 0.25% trypsin-EDTA and resuspended in DPBS containing 2% FBS. To determine GFP expression levels, 10,000 single cell events per sample were acquired on a BD LSRII flow cytometer (BD Biosciences) and analyzed using FlowJo software (TreeStar). For fluorescent microscopy analysis, complete medium was replaced with phenol red-free medium at 24 h. Cells were imaged on a Zeiss Axio Observer Z1 fluorescence microscope with an ApoTome optical sectioning attachment.

2.3 mRNA:carrier complex loading onto scaffolds

Polyplexes or lipoplexes were formed by mixing mRNA and polymer/liposome in buffer) in accordance to manufacture's protocol to a final mRNA concentration of 20 μg/mL. The polyplex/lipoplex solutions were then used to hydrate pHEMA scaffold. Some scaffolds were dip coated with uncomplexed RNA at the same concentration. Scaffolds were incubated with solutions for 4-8 h at room temperature. In a modified protocol, scaffolds were flash frozen and lyophilized after incubating with 100 μl lipoplex solution for 1h. Scaffolds were then rehydrated in another 100 μl lipoplex solution and the same incubation, lyophilization cycle was repeated for 1-4 times.

2.4 Loading efficiency and distribution of the lipoplexes

The amount of RNA loaded into the scaffolds by surface adsorption was determined by mass balance on the initial mass of RNA – mass of RNA remaining in solution after adsorption. After adsorption, the solution was mixed with equal volume of 100 mg/mL heparin and incubate for 10 min at room temperature to displace the RNA from the lipoplexes. The resultant solution was then stained with Quant-iT^{TM} RiboGreen® assay (Invitrogen) in accordance to manufacture's protocol. Fluorescence intensity was measured with plate reader and converted with standard curve into mass RNA. To visualize the distribution of lipoplexes, the cross-section of the scaffold after lipoplexes loading was imaged on a Zeiss Axio Observer Z1 fluorescence microscope with an ApoTome optical sectioning attachment.

2.5 Scaffold mediated in vitro transfection

DC 2.4 were maintained in complete medium in T75 flasks until the experiment. Cells were detached with 0.25% Trypsin-EDTA, centrifuged and resuspended in fresh medium to a concentration of 10^7 cells/mL. Lyophilized mRNA loaded scaffolds were rehydrated in complete medium for 1 h before cell seeding at 37 ˚C. After 24h culture, scaffolds along with seeded cells were fixed and imaged with a Zeiss Axio Observer Z1 fluorescence microscope with an ApoTome optical sectioning attachement using a 20x objective. Some scaffolds were also embedded in OCT compound and frozen for cryosection.

2.6 Scaffold mediated mRNA delivery in vivo

2.6.1 Study design

The experimental design used is summarized in **Table 6.2**. Six to eight week old C578L/6J female mice were anesthetized using 2% isoflurane and one scaffold per mouse was implanted subcutaneously in the dorsal right flank. For mice without scaffolds, 200 μL RNA: Stemfect™ lipoplexes were subcutaneously injected at the same location.

Table 6.2 *in vivo* scaffold based mRNA local delivery study design showing numbers of C57BL/6J female mice per experimental group. For scaffold implant groups, pHEMA or pHEMA-DM scaffolds were pre-coated with PBS, free RNA (RNA), or Stemfect™: RNA lipoplex (RNA NP) solution and were implanted subcutaneously. For mice without scaffolds, PBS, free RNA (RNA), or Stemfect™: RNA lipoplexes were subcutaneously injected at the same location.

Delivery method	RNA NP	RNA	PBS
pHEMA scaffolds	3	3	1
pHEMA-DM scaffolds	3	3	1
No scaffold, s.c. injection	3	3	1

2.6.2 In vivo mRNA distribution

mRNA was labeled with Cy5 using a *Label*IT Tracker Kit (MirusBio) at a 0.5 v/w ratio of *Label*IT Tracker Reagent to mRNA in accordance with the manufacturer's protocol. Mice were anesthetized with isoflurane, and imaged for Cy5 fluorescence using a Xenogen IVIS200 Spectrum Imager. Image analysis was performed using Living Image software (Caliper).

2.6.3 Local mRNA uptake and transgene expression

At 72 h post-implantation/injection, animals were euthanized by CO_2. Implants along with the adjacent skin tissue were excised and imaged with Xenogen IVIS200 Spectrum Imager for GFP expression. Following this, the explants were digested with and the ingrown tissue was digested

into single cell suspensions using a collagenase solution (Worthington, 250 U/mL) that was agitated at 37 ˚C for 45min. The cell suspensions were then poured through a 40 μm cell strainer to isolate cells from scaffold debris. Cells were then stained with Pacific Blue-anti-CD11c (BioLegend, San Diego, CA) analyzed by flow cytometry.

2.6.4 Lipoplex trafficking to draining lymph nodes

Animals were euthanized by CO_2 and the inguinal lymph nodes were isolated. Lymph nodes were digested with Collagenase II And 2 mg/mL DNAseI (Roche, Indianapolis, IN), filtered through a 40 μm cell strainer, and incubated for 5 min in ACK buffer to lyse erythrocytes. Cell suspensions were incubated with rat anti-mouse CD16/32 antibody (BD Biosciences, San Jose, CA) to block Fc receptors, then stained with Pacific Blue-anti-CD11c (BioLegend, San Diego, CA). Approximately 100,000 single cell events per sample were collected using a BD LSRII and analysed using FlowJo software (TreeStar).

3. Results

3.1 mRNA formulation on size and transfection capacity

Since mRNA is prone to degradation at room temperature and lipoplexes are reported to be unstable in liquid suspension(Anchordoquy, Carpenter, & Kroll, 1997). A method of combining high concentration mRNA lipoplexes solution and lyophilization was used in the study to reduce the incubation time, enhance loading efficiency, and improve long term stability of the mRNA. Lyoprotectant trehalose was incorporated in the lipoplex formulation to prevent particle aggregation and to retain mRNA functionality during lyophilization cycles. The particle size was

measured 10 min post forming lipoplexes and after each lyophization and rehydration cycle. While the addition of 250 mM trehalose solution did not affect the particle size immediately after lipoplex formation, it significantly prevented particle aggregation during lyophilization cycles (**Figure 6.1**). Lipoplexes formulated with trehalose retained an average size of <300 nm after the first two lyophilization cycles, and <500 nm after the third cycle. In contrast, formulation without any lyoprotectant quickly aggregated into particles which size are averaged to be ~ 2 μm after the first lyophilization rehydration cycle.

To investigate how the functionality of the mRNA lipoplexes correlates to the size change, their bioactivity was evaluated by *in vitro* transfection of BHK cells (**Figure 6.2**). As indicated by results, the increase in particle size lead to rapid decrease in the lipoplexes capacity to mediate mRNA transfection. Without lyoprotectant the mRNA lipoplexes lost over 90% transfection efficiency after the first freeze dry cycle. In contrast, with the addition of trehalose the particles retained 80% and 65% of transfection capacity after 2 and 3 freeze drying cycles compared with freshly prepared particles, respectively.

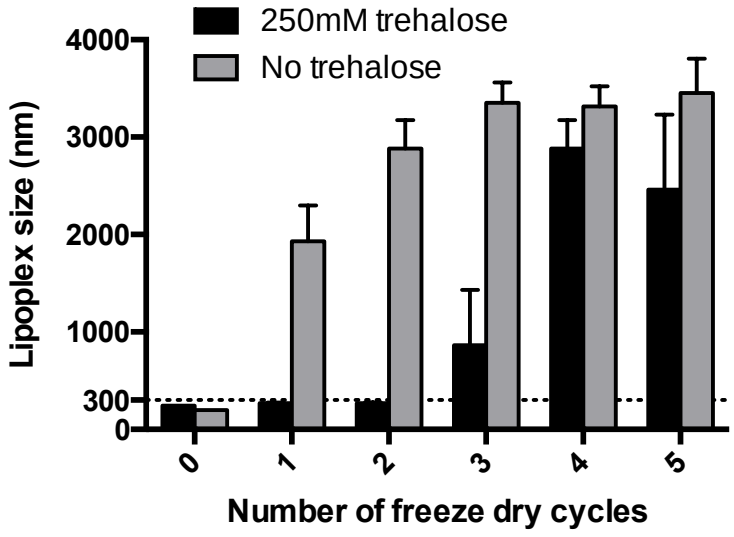

Figure 6.1 Effect of lyoprotectant and freeze dry cycle on lipoplex sizes.

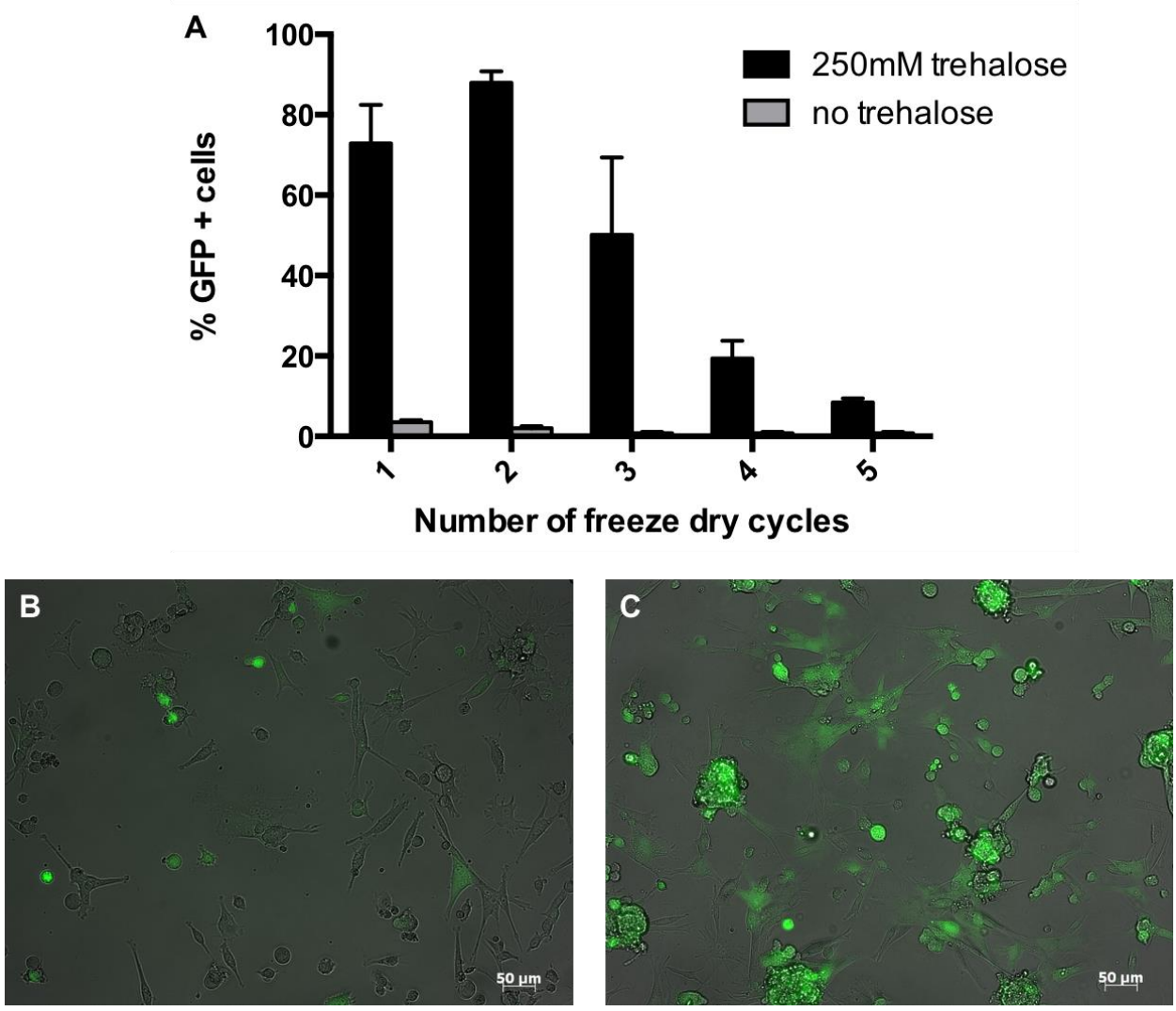

Figure 6.2 Effect of trehalose addition and freeze dry cycle on BHK cell transfection. Top: Transfection efficiency of Stemfect™ lipoplexes after each freeze dry cycle. Bottom: BHK cells transfected with Stemfect™ lipoplexes formulated (A), without trehalose; (B) with trehalose, after lyophilization cycle once.

3.2 Loading efficiency and lipoplex distribution

To evaluate the adsorption efficiency on both HEMA and HEMA-DM scaffolds at various time points, the un-adsorbed mRNA remained in the solution was extracted with heparin and stained with Ribogreen stain and quantified with Ribogreen® assay in accordance with the manufacturer's protocol.

First, the physical adsorption of mRNA: *in vivo*-jetPEI polyplexes or mRNA: Stemfect™ lipoplexes solution onto pHEMA or pHEMA-DM scaffolds was tested. DM modified HEMA scaffold exhibited excellent ability to adsorb polymer-based carriers that contain several amine groups that can form covalent bonds with the catechol groups on DM monomers. Over 85% mRNA polyplexes in solution were adsorbed on HEMA-DM scaffolds after 2 h incubation (**Figure 6.3**). Since most lipid based carriers do not contain end groups that can readily react with catechol groups on DM or hydroxyl groups on HEMA, only 40-50% of the total lipid based nanoparticles(lNP) in solution was deposited on the surface of the scaffolds after 4 h incubation. Moreoever, the distribution of mRNA complexes throughout incubation in solution is mostly concentrated on the outer superficial layers of the scaffolds. (**Figure 6.4, A**)

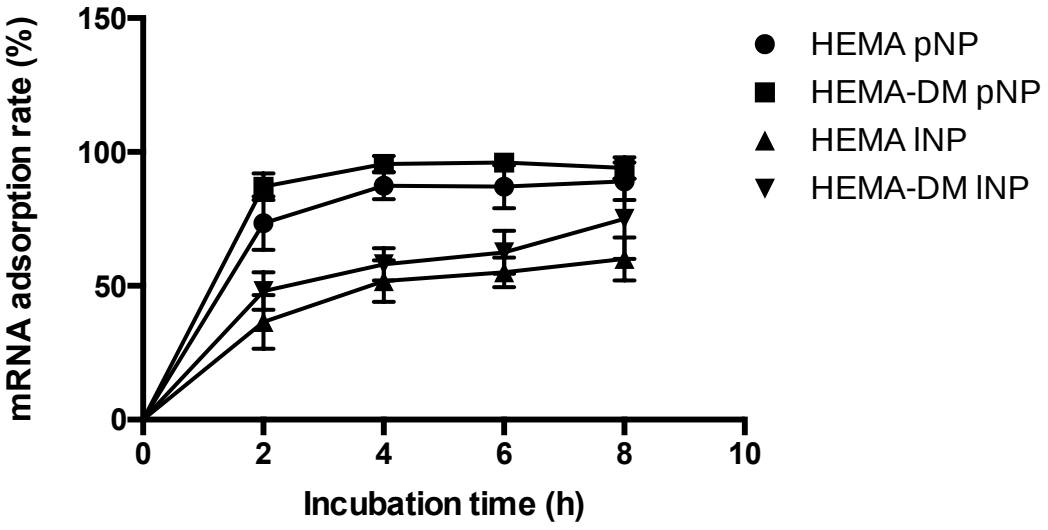

Figure 6.3 Adsorption efficiency. Experiment include pHEMA scaffold with mRNA/*in vivo*-jetPEI polyplexes (HEMA pNP), pHEMA-DM scaffold with mRNA/*in vivo*-jetPEI polyplexes (HEMA-DM pNP), pHEMA scaffold with mRNA/Stemfect™ lipoplexes (HEMA lNP), and pHEMA-DM scaffold with mRNA/Stemfect™ lipoplexes (HEMA-DM lNP).

Since lipid based Stemfect™ does not contain amine groups that can react with DM modified HEMA, a lyophilization-rehydration protocol was developed to improve the coating efficiency of

lipoplexes. When loading mRNA lipoplexes onto scaffolds using the lyophilization procedure for 2 h incubation, 83.7 ± 9.2 % mRNA adhered to the scaffold regardless of the type of carrier used. Also, the lyophilization process lead to a more even distribution throughout the scaffold (**Figure 6.4, B**).

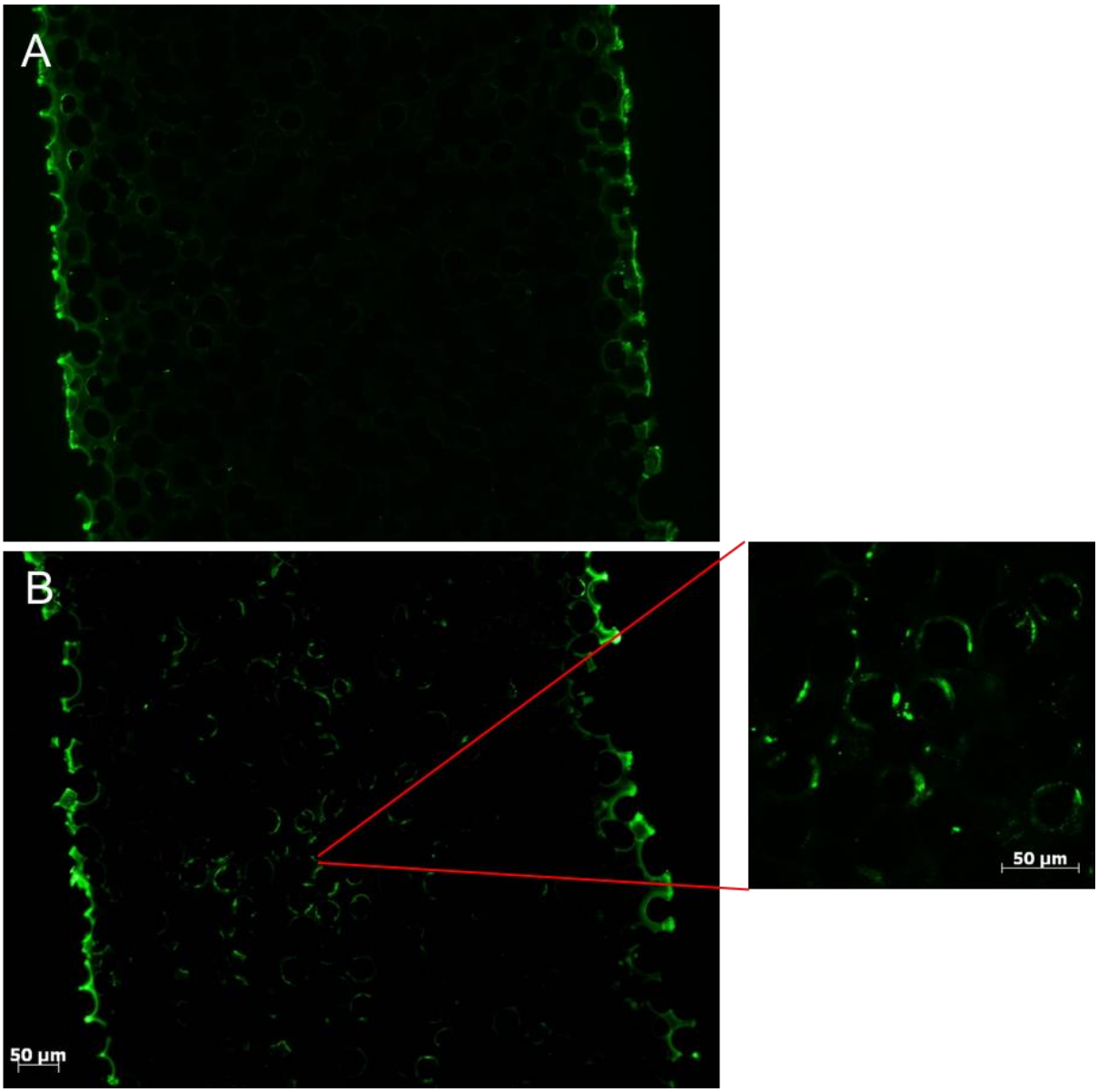

Figure 6.4 mRNA lipolexes distribution in pHEMA scaffolds. mRNA was labeled with YOYO-1. mRNA lipoplexes loading through (**A**) co-incubation with mNRA solution, (**B**) incubation with mRNA solution followed by lyophilization. (**A**) (**B**) scale bar = 50 µm

3.3 in vitro transfection of mRNA loaded scaffolds

An *in vitro* scaffold mediated mRNA transfection was performed using DC2.4 murine dendritic cells. Lipoplexes were loaded onto scaffolds with lyophilization-rehydration method as described in Chapter 6, section 2.3. While lipoplexes formulated without lyoprotectant did not facilitate any mRNA transfection upon adsorption and lyophilization process, trehalose formulated mRNA successfully transfected DC2.4 cells seeded within the scaffold. Cross-section images of the scaffold documents Cy5 labeled uptake and the spatial distribution of transfected cells (**Figure 6.5, C, D**). While the seeding procedure allowed cell infiltration throughout the scaffold, most of the mRNA uptake and GFP protein expression was observed on the outer scaffold layers. Overall, these results indicate that lipoplexes adsorbed on HEMA scaffolds retained the capacity to mediate mRNA intracellular transfection.

3.4 In vivo imaging of mRNA vector distribution

Live animal imaging was used to monitor the distribution of fluorescent Cy5-tagged mRNA within polyplexes. In a pilot study, sr-mRNA-GFP was formulated with *in vivo*-jetPEI and loaded on pHEMA and pHEMA-DM scaffolds through surface adsorption. Consistent with adsorption efficiency results, higher amounts of Cy5-sr-mRNA was detected from HEMA-DM scaffolds than HEMA scaffolds upon implantation (**Figure 6.6**). Throughout the 2-week tracking, mRNA release and distribution remained local at the implantation site. Intriguingly, both the mRNA signal and GFP expression re-intensified again at Day 9 through Day 13. sr-mRNA polyplexes adsorbed on both HEMA-DM and HEMA scaffolds demonstrated sustained local RNA release. Higher adsorption efficiency on the HEMA-DM scaffolds resulted in an overall stronger mRNA signal.

Further *in vivo* studies were focused on ss-mRNA complexes using lipid-based carriers which demonstrated better transfection efficiency (see **Chapter 5**). pHEMA scaffolds loaded with Cy5

labeled ss-mRNA-GFP (lipoplexes or free mRNA) were implanted in mice as described. Naked mRNA in solution was administered to mice via subcutaneous injection for comparison (**Figure 6.7**). Consistent with our previous hypothesis, mRNA delivered from scaffolds exhibited prolonged release compared to bolus delivery. 24 h and 72 post implantation/injection, the amount of Cy5-labeled mRNA retained on scaffolds is more than 3 times what is retained at a injection site. Also, at each time point, RNA lipoplexes groups have 2.5 to 6.7 times stronger signals than their unformulated free mRNA controls, suggesting lipoplexes successfully protected mRNA from degradation and improved stability *in vivo*.

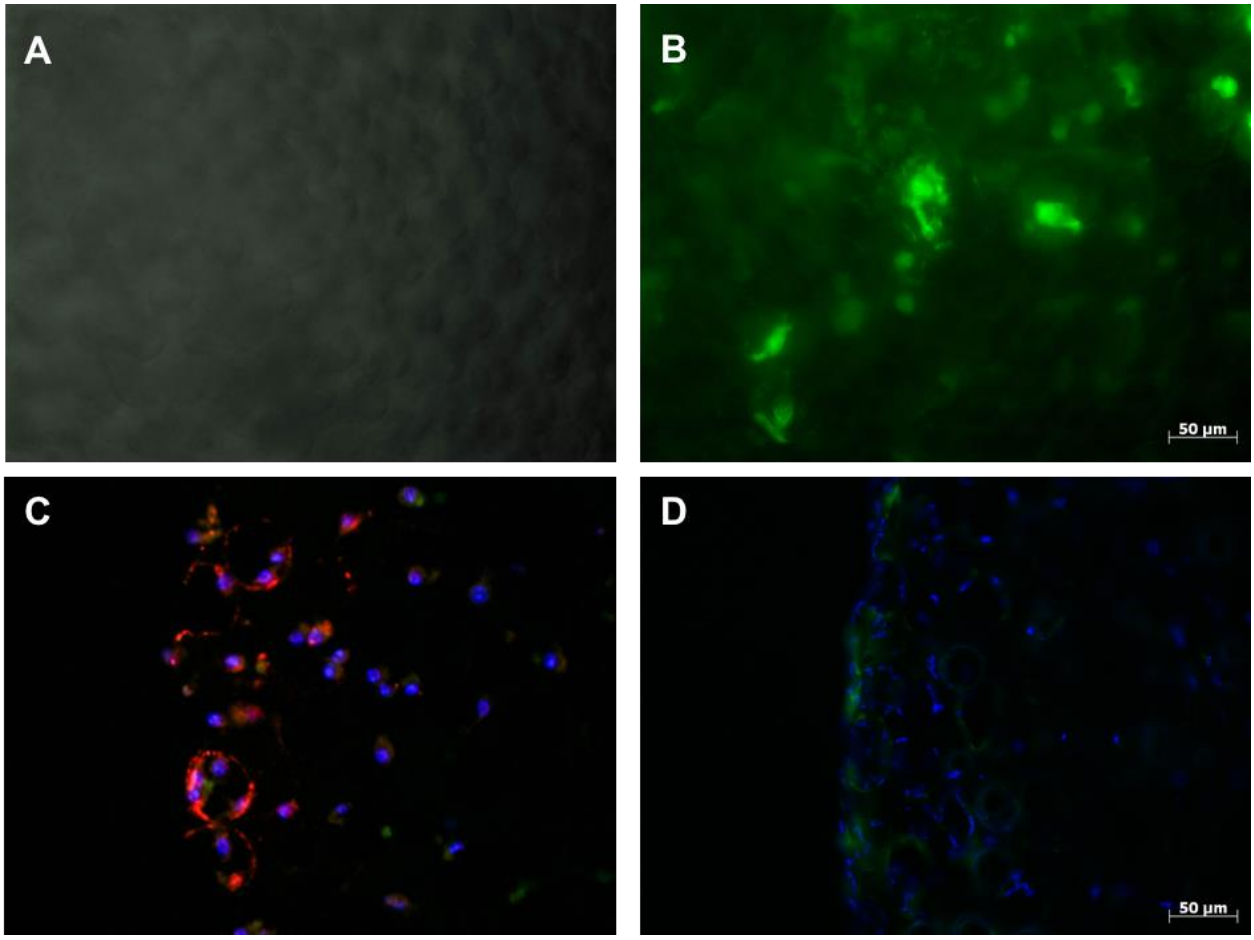

Figure 6.5 DC2.4 transfection on pHEMA scaffolds. (**A**) no mRNA control, (**B**) DC2.4 24h post transfection. Cross-section images of pHEMA scaffold after DC2.4 transfection (**C**) Cy5 labeled mRNA uptake, (**D**) GFP expression. Cell nucleus was stained with DAPI in **C** and **D**. Scale bar is 50 µm.

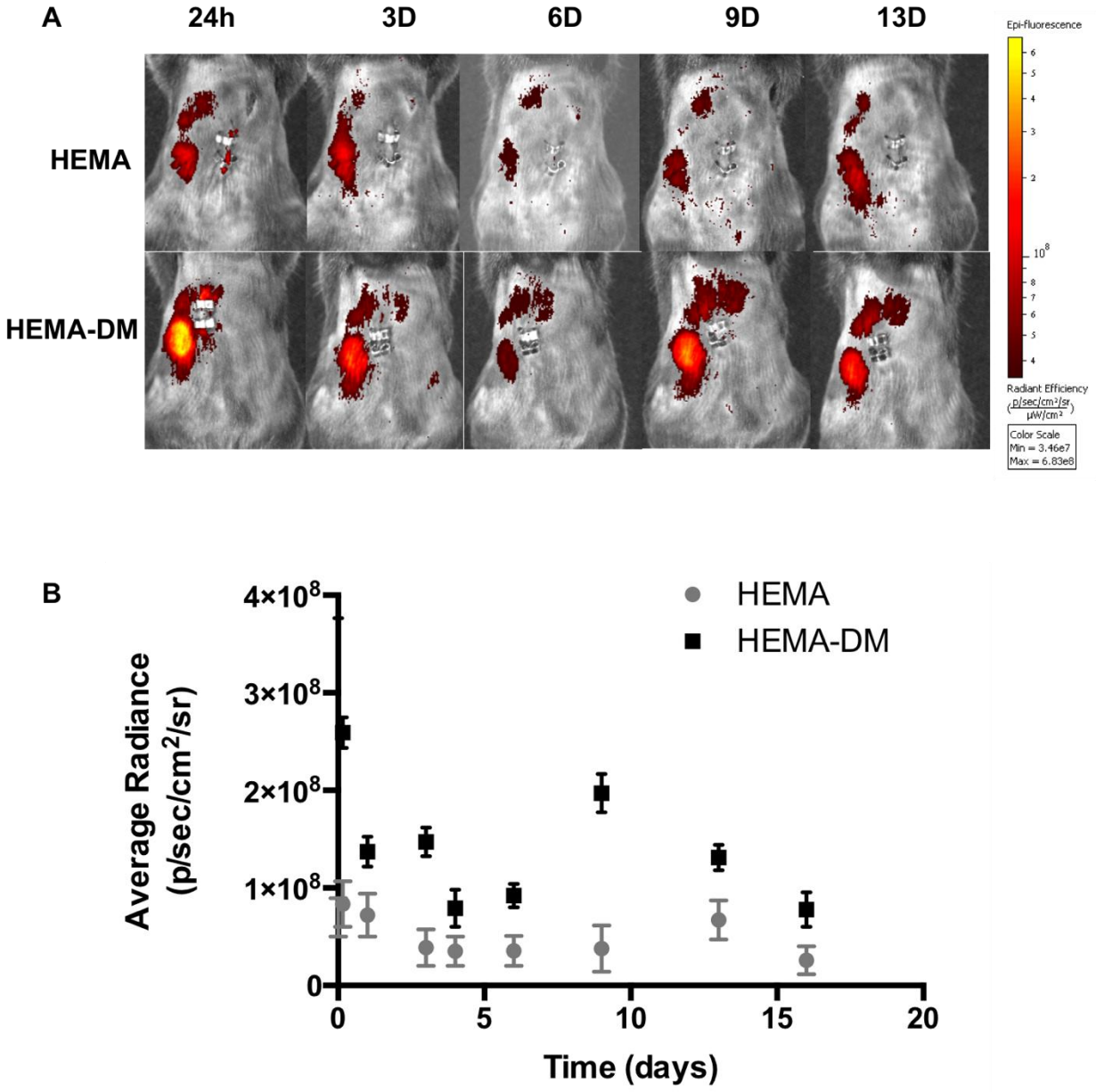

Figure 6.6 IVIS imaging and quantification of Cy-5 labeled sr-mRNA. (**A**) IVIS imaging over the course of two weeks of the distribution of Cy5-labeled sr-mRNA/*in vivo*-jetPEI loaded on Top: HEMA; Bottom: HEMA-DM scaffold. (**B**) Average Cy5 fluorescence signal measured by IVIS.

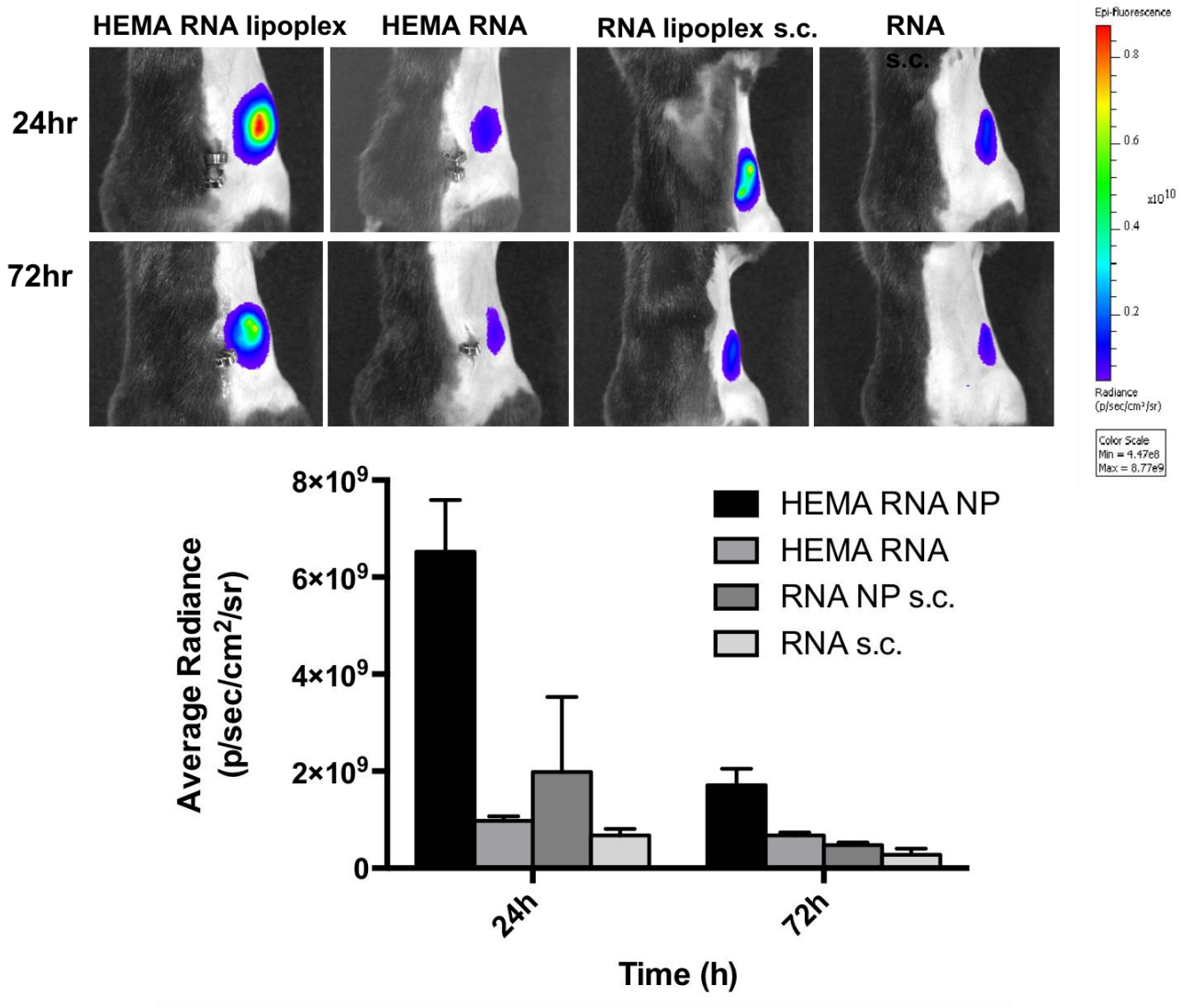

Figure 6.7 *In vivo* distribution and quantitation of Cy5 labeled mRNA. **Top**: IVIS imaging on Day1 and Day3. Mice were either implanted with HEMA scaffolds loaded with free mRNA or Stemfect^{TM} formulated lipoplexes, or received the same amount of mRNA via subcutaneous injection; **Bottom**: Average Cy5 fluorescence signal measured by IVIS.

3.5 Scaffold mediated in vivo transfection of mRNA

To investigate if higher mRNA local retention leads to higher transfection efficiency, local GFP expression was evaluated between scaffolds and/or skin tissue explants. 24h post implantation/injection, GFP expression was detected on both scaffold groups (free or formulated mRNA), whereas almost no signal was detected from either bolus delivery group. At Day 3, similar level GFP expression was detected from scaffold mediated delivery, indicating sustained GFP expression was achieved with scaffold mediated delivery of mRNA. Flow cytometry analysis of cells extracted from the implants and adjacent skin showed both scaffold-based local delivery and lipoplex formulation lead to enhanced and more persistent mRNA uptake (**Figure 6.9**). 15% cells analyzed from HEMA lipoplex group showed Cy5(+) mRNA uptake, in comparison to 6% from bolus delivery group. However, no improved DC recruitment was observed at the implantation site with the addition of mRNA vectors. No DC specific transfection or lymph node homing was detected either.

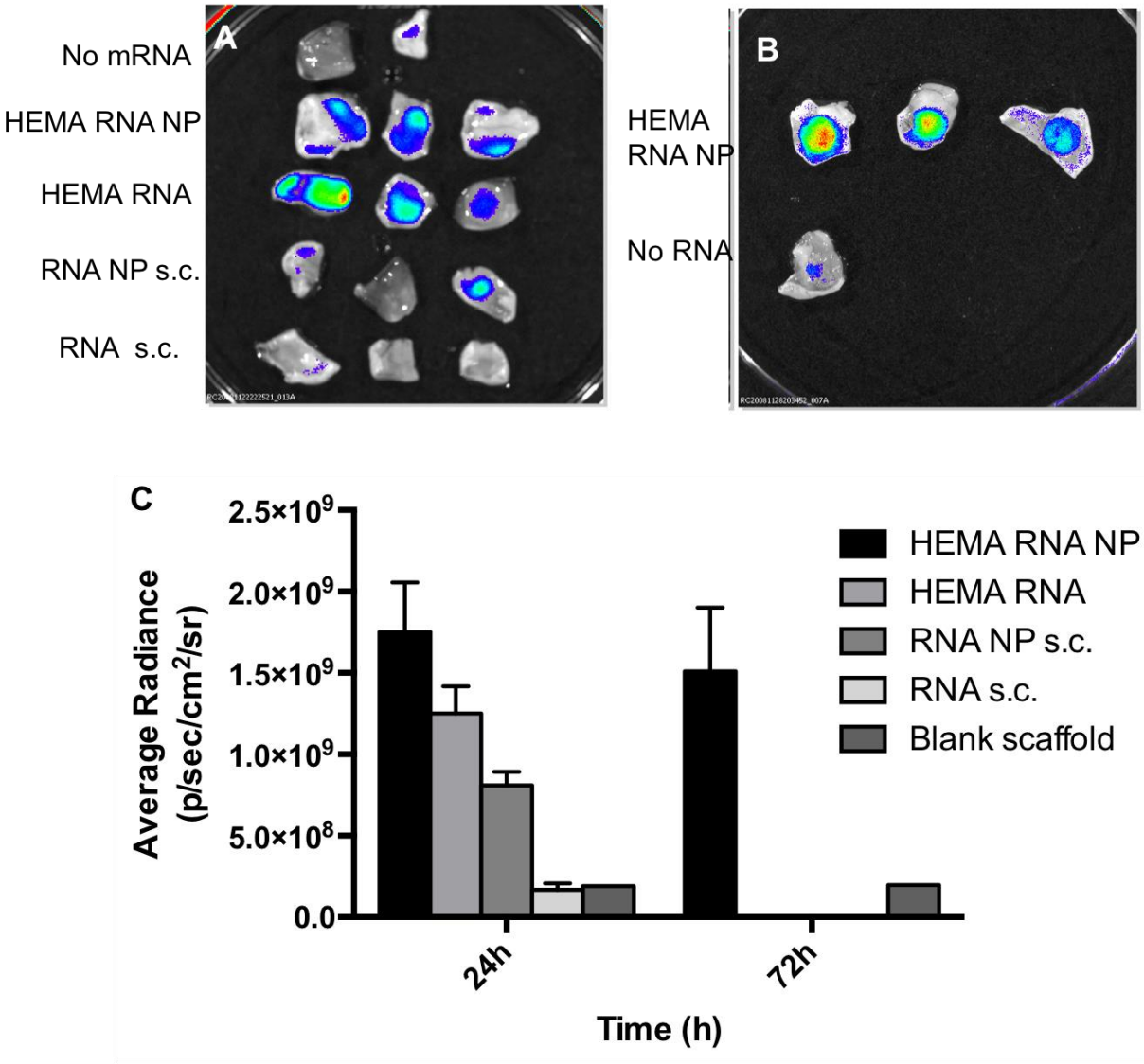

Figure 6.8 IVIS imaging and quantitation of local GFP expression from scaffolds and adjacent skin tissue. Experimental groups include HEMA scaffold control (no mRNA/blank scaffold), HEMA scaffold with mRNA/Stemfect™ lipoplexes (HEMA RNA NP), HEMA scaffold with free mRNA (HEMA RNA), mRNA/Stemfect™ subcutaneous bolus injection (RNA NP s.c.), and free mRNA subcutaneous bolus injection (RNA s.c.).

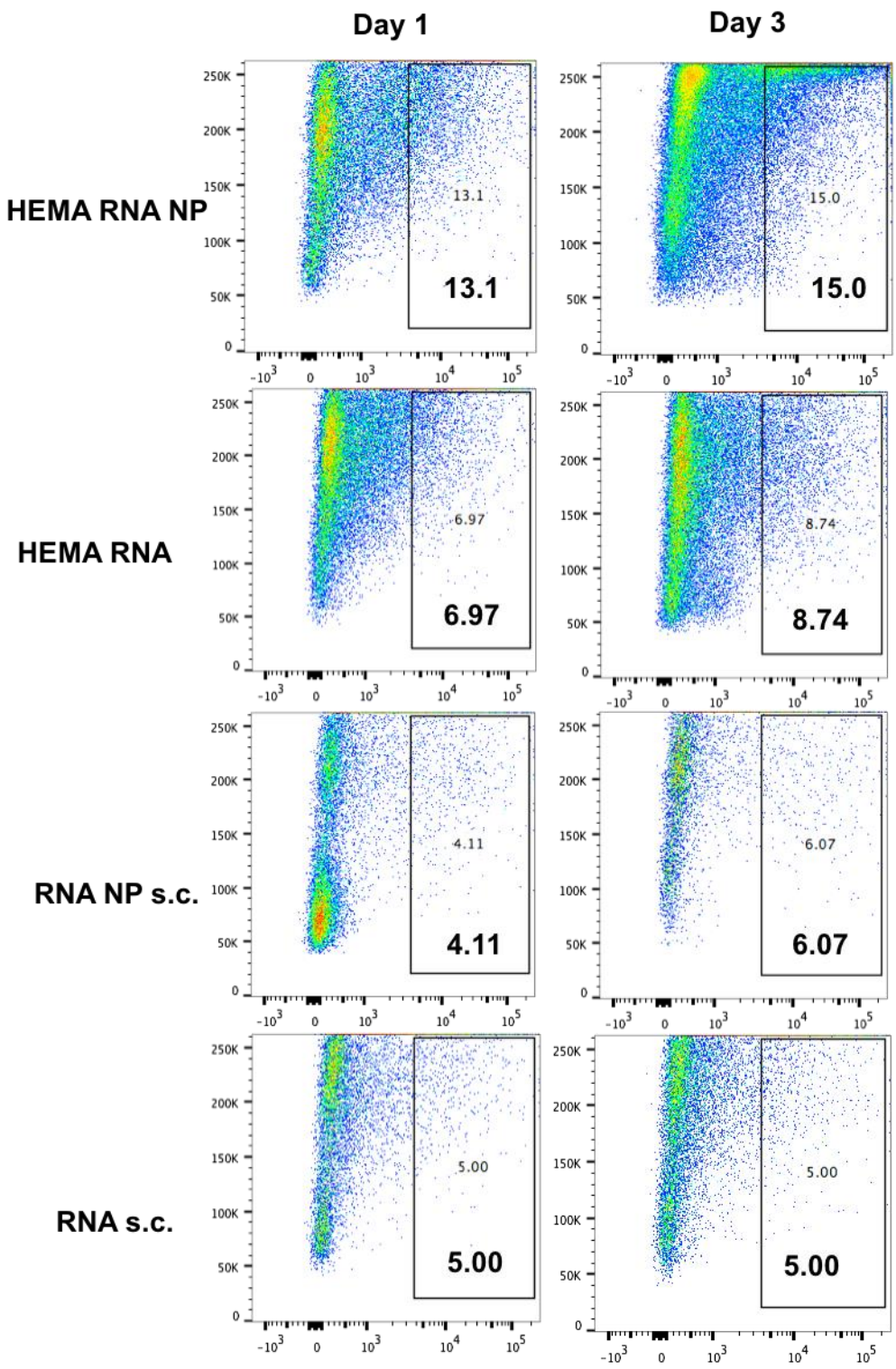

Figure 6.9 Local uptake of Cy5 labeled mRNA on Day 1 and Day 3 analyzed by flow cytometry. Displayed experimental groups include HEMA scaffold with mRNA/Stemfect^{TM} lipoplexes (HEMA RNA NP), HEMA scaffold with free mRNA (HEMA RNA), mRNA/Stemfect^{TM} subcutaneous bolus injection (RNA NP s.c.), and free mRNA subcutaneous bolus injection (RNA s.c.).

4. Discussion

pHEMA scaffolds were selected for the mRNA local delivery platform due to better long term tissue integration and vascularization as described in Chapter 4. We modified pHEMA scaffolds for the immobilization of PEI based polyplexes, since PEI was considered efficient at DNA transfection and widely applied to many nucleic acid delivery systems. Dopamine methacrylamide (DM) modified HEMA contains catechol groups that can readily form covalent bonds with amine groups through Schiff base reaction or Michael addition. Results indicated faster and more efficient PEI polyplexes adsorption was achieved using dopamine modified scaffolds. Dopamine modification of scaffolds can be used to immobilize many biomolecules if they contain amine groups. As our *in vitro* study revealed, lipid based carriers were more efficient at mRNA delivery. Different strategies to improve physical adsorption or embedding of the lipoplexes were explored, including copolymerize HEMA with negatively charged methacrylic acid or applying thin coatings of fibrin/lipoplex mixture over the surface of scaffold. While a negatively charged surface greatly improved loading efficiency, the amount of charge required induced significant cytotoxicity and swelling *in vivo*. Conversely, fibrin coating rendered a soft layer on the scaffold surface that was not uniform. While some experiments with fibrin-coated scaffold received positive results, the overall consistency was poor. Consequently, a series of physical adsorption of mRNA:liposome lipoplexes followed with a lyophilization step was used for mRNA loading. While this is a common method used to load therapeutics onto scaffolds, additional optimization was needed for mRNA lipoplexes, which are prone to degradation and aggregation. The use of lyoprotectant such as glucose and trehalose was previously reported in many literature (Anchordoquy et al., 1997; Yadava, Gibbs, Castro, & Hughes, 2008). In this study, the addition of trehalose successfully maintained mRNA bioactivity during incubation and lyophilization cycles.

After demonstrating *in vitro* transfection with lipoplex-loaded scaffolds, a mice model was used to evaluate the mRNA distribution and transgene expression *in vivo*. Consistent with what we previously hypothesized, both vector release platform (injection vs. scaffold) and liposome formulation played important roles in promoting sustained local release and expression.

While transgene expression was observed in the explant, the level of expression was lower than local mRNA release and uptake. This may indicate mRNA degradation on the scaffold *in vivo*. While mRNA is usually considered more stable in the subcutaneous space, potential cell and protein adhesion onto the scaffold may create an environment with more nuclease activity. Although transgene expression was captured with IVIS, flow analysis showed a low population of GFP+ cells (<1%). By comparing explant GFP images with the Cy5 signal imaged within the same samples; while mRNA release extended beyond the scaffolds, transgene expression was mostly concentrated on the implants. This suggests a possible bias of the flow analysis due to different cell extraction efficiencies from the tissues and the scaffolds. While the same method was applied to extract cells from polymeric scaffolds in previous literature(O. a Ali et al., 2009), the efficiency of such method was not mentioned. So further studies need to be performed to validate the cell extraction protocol. Alternatively, a strategy to analyze cell transfection *in situ* is required.

5. Conclusion

We demonstrated that mRNA lipoplexes formulated with lyoprotectant trehalose were protected from aggregating and loss of bioactivity during lyophilization process. Lipoplexes were loaded onto scaffolds via surface adsorption. Scaffold mediated transfection was first demonstrated *in vitro* successfully. Scaffolds loaded with lipoplexes or free mRNA were implanted in mice subcutaneously. Their mRNA distribution and ability to induce mRNA uptake and transgene

expression were assessed and compared with subcutaneous bolus delivery. Results demonstrated that both liposome formulation and local immobilization of mRNA via scaffolds were important to mRNA sustained delivery and transfection, and scaffold based delivery resulted Lipoplexes loaded scaffolds exceled other control groups (naked RNA loaded scaffolds and subcutaneous injections) in all aspects including prolonged local release of mRNA, improved local mRNA uptake by cells, and increased GFP transgene expression at implantation site. These results demonstrated that scaffold-based delivery have advantages over bolus delivery and can be potentially used as an mRNA therapeutics delivery platform.

Chapter 7 Conclusions, limitations, and future directions

Biomaterials have been used widely for tissue engineering and drug delivery applications. More recently, biomaterial platforms have emerged as a promising option for vaccine delivery. Implantable biomaterials serve a dual purpose of (a) controlled release of therapeutics and (b) immune cell modulation. The goal of this work was to develop a porous scaffold platform as a novel strategy for mRNA vaccine local delivery. Biomaterial scaffolds of specific material and pore size was expected to promote DCs accumulation and maturation at implantation site.

In our *in vitro* studies, we observed that a smaller pore size was more favorable for DC maturation, which is characterized by secretion of pro-inflammatory cytokines, and upregulation of maturation and co-stimulatory molecules. *In vivo* implantation further revealed that scaffolds of smaller pore sizes promoted CD11c (+) DCs accumulation and upregulation of maturation markers CD86 and MHCII at implantation site in the first week post-immunization. Scaffold adjuvant effects to the co-delivered OVA protein was assessed. While scaffolds adjuvant demonstrated limited ability at promoting cellular response *in vivo*, enhanced humoral response characterized by antigen specific antibodies production was observed in the first two weeks. Similar to what's observed *in vitro*, scaffolds with smaller pore lead to higher level DC recruitment and maturation *in vivo*. Also, a throat size >10 μm was noted to be essential to guarantee sufficient cell infiltration into scaffolds. Overall, our results demonstrated that 40 μm pHEMA scaffolds is ideal for a local vaccine delivery platform.

Scaffold based gene therapies have been limited to pDNA, siRNA and miRNA so far, all of which are considered to be more stable than ss-mRNA. mRNA delivery *in vivo* has been carried out by various approaches, most of which are systemic delivery routes that lead to transient expression. Repeated administrations were necessary to induce immune response. To our knowledge, there has not been any study demonstrating sustained mRNA delivery from implantable scaffolds.

mRNA delivery to slow dividing cells such as DCs *in vivo* has always been a challenge to the development of nucleic acid vaccines. Since antigen uptake and processing by DC is a prerequisite to T cell priming and adaptive immunity initiation, a series of polymer and lipid based carriers were evaluated for their capacity to mediate mRNA transfection in various cell types. Lipoplexes formed with Stemfect^{TM} demonstrated superior capacity in facilitating intracellular mRNA delivery across a variety of cell lines especially dendritic cells while maintaining excellent cell viability, demonstrating the potential to be used in mRNA-based vaccine application.

Scaffolds loaded with free mRNA or lipoplexes were implanted in the dorsal region of mice model subcutaneously. They were compared with subcutaneous bolus injection with the same dosage and formulation. In 72 h duration post implantation, lipoplexes loaded scaffolds demonstrated stronger and prolonged local signal of mRNA, enhanced mRNA uptake, and higher transgene expression at the implantation site. However, no DC specific transfection or lymph node homing was observed. We had previously hypothesized that scaffolds with optimal pore size might be able to promote sufficient DC accumulation and maturation for enhanced mRNA uptake and lymph node homing, but our findings indicate that other key components in scaffold design are needed.

In future studies, the scaffold vaccine delivery platform can be improved by incorporating other cytokines and adjuvants such as GM-CSF, CpG, and poly I:C, to enrich DCs recruitment and induce specific phenotypes. sr-mRNA also holds great potential as an alternative to ss-mRNA. It

is believed that the self-amplifying nature of sr-mRNA is ideal for quiescent cell transfection and sustained local release, offsetting the loss of efficiency due to degradation *in vivo*. In this study, we have proven enhanced transfection in BHK cell lines and prolonged mRNA signal (> 2 weeks) *in vivo*. Based on these promising findings, we believe that sr-mRNA derived from a non-cytopathic virus strain merits further investigation in order to fully explore its potential in scaffold based vaccine delivery platform.

References

Acharya, A. P., Dolgova, N. V., Clare-Salzler, M. J., & Keselowsky, B. G. (2008). Adhesive substrate-modulation of adaptive immune responses. *Biomaterials*, *29*(36), 4736–4750.

Agapov, E. V, Frolov, I., Lindenbach, B. D., Prgai, B. M., Schlesinger, S., Rice, C. M., & Ahlquist, P. (1998). Noncytopathic Sindbis virus RNA vectors for heterologous gene expression. *Cell Biology*, *95*(22), 12989–12994.

Alexopoulou, L., Czopik Holt, A., Medzhitov, R., & Flavell, R. A. (2001). Recognition of double-stranded RNA and activation of NF-kappa B by Toll-like receptor 3. *Nature*, *413*(6857), 732–738.

Ali, O. A., & Mooney, D. J. (2008). Sustained GM-CSF and PEI condensed pDNA presentation increases the level and duration of gene expression in dendritic cells. *Journal of Controlled Release*, *132*(3), 273–278.

Ali, O. a, Huebsch, N., Cao, L., Dranoff, G., & Mooney, D. J. (2009). Infection-mimicking materials to program dendritic cells in situ. *Nature Materials*, *8*(2), 151–158.

Anchordoquy, T. J., Carpenter, J. F., & Kroll, D. J. (1997). Maintenance of transfection rates and physical characterization of lipid/DNA complexes after freeze-drying and rehydration. *Archives of Biochemistry and Biophysics*, *348*(1), 199–206.

Babensee, J. E. (2008). Interaction of dendritic cells with biomaterials. *Seminars in Immunology*, *20*(2), 101–108.

Babensee, J. E., & Paranjpe, A. (2005). Differential levels of dendritic cell maturation on different biomaterials used in combination products. *Journal of Biomedical Materials Research - Part*

A, *74*(4), 503–510.

Banchereau J, S. R. (1998). Dendritic cells and the control of immunity. *Nature.*, *19*(392), 245–252.

Banerjee, P., Biswas, A., & Biswas, T. (2008). Porin-incorporated liposome induces Toll-like receptors 2- and 6-dependent maturation and type 1 response of dendritic cell. *International Immunology*, *20*(12), 1551–1563.

Bennewitz, N. L., & Babensee, J. E. (2005). The effect of the physical form of poly(lactic-co-glycolic acid) carriers on the humoral immune response to co-delivered antigen. *Biomaterials*, *26*(16), 2991–2999.

Bernstein, D. I., Reap, E. A., Katen, K., Watson, A., Smith, K., Norberg, P., … Chulay, J. D. (2009). Randomized, double-blind, phase 1 trial of an alphavirus replicon vaccine for cytomegalovirus in CMV seronegative adult volunteers. *Vaccine*, *28*(2), 484–493.

Bettinger, T., Carlisle, R. C., Read, M. L., Ogris, M., & Seymour, L. W. (2001). Peptide-mediated RNA delivery: a novel approach for enhanced transfection of primary and post-mitotic cells. *Nucleic Acids Research*, *29*(18), 3882–3891.

Boczkowski, D., Nair, S. K., Nam, J. H., Lyerly, H. K., & Gilboa, E. (2000). Induction of tumor immunity and cytotoxic T lymphocyte responses using dendritic cells transfected with messenger RNA amplified from tumor cells. *Cancer Research*, *60*(4), 1028–1034.

Bonifaz, L. C., Bonnyay, D. P., Charalambous, A., Darguste, D. I., Fujii, S.-I., Soares, H., … Steinman, R. M. (2004). *In Vivo* Targeting of Antigens to Maturing Dendritic Cells via the DEC-205 Receptor Improves T Cell Vaccination. *The Journal of Experimental Medicine*,

38151000(6), 815–824.

Breckpot, K., Aerts, J. L., & Thielemans, K. (2007). Lentiviral vectors for cancer immunotherapy: transforming infectious particles into therapeutics. *Gene Therapy*, *14*(11), 847–862.

Carroll, T. D., Matzinger, S. R., Barro, M., Fritts, L., McChesney, M. B., Miller, C. J., & Johnston, R. E. (2011). Alphavirus replicon-based adjuvants enhance the immunogenicity and effectiveness of Fluzone ® in rhesus macaques. *Vaccine*, *29*(5), 931–940.

Caux, C., Vanbervliet, B., Massacrier, C., Ait-Yahia, S., Vaure, C., Chemin, K., … Vicari, A. (2002). Regulation of dendritic cell recruitment by chemokines. *Transplantation*, *73*(1), S7-11.

Corinti, S., Albanesi, C., la Sala, A., Pastore, S., & Girolomoni, G. (2001). Regulatory activity of autocrine IL-10 on dendritic cell functions. *The Journal of Immunology*, *166*(7), 4312–4318.

Démoulins, T., Milona, P., Englezou, P. C., Ebensen, T., Schulze, K., Suter, R., … Mccullough, K. C. (2016). Polyethylenimine-based polyplex delivery of self-replicating RNA vaccines. *Nanomedicine: Nanotechnology, Biology and Medicine*, *12*(3), 711–722.

Diebold, S. S., Kaisho, T., Hemmi, H., Akira, S., & Sousa, C. R. e. (2004). Innate antiviral responses by means of TLR7-mediated recognition of single-stranded RNA. *Science*, *303*(5663), 1529–1531.

Dieu-Nosjean, M. C., Vicari, A., Lebecque, S., & Caux, C. (1999). Regulation of dendritic cell trafficking: a process that involves the participation of selective chemokines. *Journal of Leukocyte Biology*, *66*(2), 252–262.

Dryga, S., Dryga, O., & Schlesinger, S. (1997). Identification of mutations in a Sindbis virus

variant able to establish persistent infection in BHK cells: the importance of a mutation in the nsP2 gene. *Virology*, *228*(228), 74–83.

Galperin, A., Oldinski, R. A., Florczyk, S. J., Bryers, J. D., Zhang, M., & Ratner, B. D. (2013). Integrated bi-layered scaffold for osteochondral tissue engineering. *Advanced Healthcare Materials*, *2*(6), 872–883.

Geall, A. J., Mandl, C. W., & Ulmer, J. B. (2013). RNA: The new revolution in nucleic acid vaccines. *Seminars in Immunology*, *25*(2), 152–159.

Geall, A. J., Verma, A., Otten, G. R., Shaw, C. A., Hekele, A., Banerjee, K., … Mandl, C. W. (2012). Nonviral delivery of self-amplifying RNA vaccines. *Proceedings of the National Academy of Sciences of the United States of America*, *109*(36), 14604–14609.

Godbey, W. T., Wu, K. K., & Mikos, A. G. (1999). Poly(ethylenimine) and its role in gene delivery. *Journal of Controlled Release*, *60*, 149–160.

Hartman, B. H., Reh, T. A., & Bermingham-McDonogh, O. (2010). Notch signaling specifies prosensory domains via lateral induction in the developing mammalian inner ear. *Proceedings of the National Academy of Sciences of the United States of America*, *107*(36), 15792–15797.

Heil, F., Hemmi, H., Hochrein, H., Ampenberger, F., Kirschning, C., Akira, S., … Bauer, S. (2004). Species-specific recognition of single-stranded RNA via toll-like receptor 7 and 8. *Science*, *303*(5663), 1526–1529.

Heit, A., Busch, D. H., Wagner, H., & Schmitz, F. (2008). Vaccine protocols for enhanced immunogenicity of exogenous antigens. *International Journal of Medical Microbiology*,

298(1–2), 27–32.

Huang, H., Ostroff, G. R., Lee, C. K., Specht, C. A., & Levitz, S. M. (2010). Robust stimulation of humoral and cellular immune responses following vaccination with antigen-loaded β-Glucan particles. *mBio*, *1*(3), e00164-10.

Iribarren, P., Correa, S. G., Sodero, N., & Riera, C. M. (2002). Activation of macrophages by silicones: phenotype and production of oxidant metabolites. *BMC Immunology*, *3*(1), 1–6.

Jang, J. J.-H., Bengali, Z., Houchin, T. L., & Shea, L. D. (2006). Surface adsorption of DNA to tissue engineering scaffolds for efficient gene delivery. *Journal of Biomedical Materials Research Part A*, *77A*(1), 50–58.

Kapsenberg, M. L. (2003). Dendritic-cell control of pathogen-driven T-cell polarization. *Nature Reviews Immunology*, *3*(12), 984–993.

Kim, J., Li, W. A., Sands, W., & Mooney, D. J. (2014). Effect of pore structure of macroporous poly(lactide-co-glycolide) scaffolds on the *in vivo* enrichment of dendritic cells. *ACS Applied Materials and Interfaces*, *6*(11), 8505–8512.

Kleindienst, P., & Brocker, T. (2003). Endogenous dendritic cells are required for amplification of T cell responses induced by dendritic cell vaccines *in vivo*. *J.Immunol.*, *170*(0022–1767), 2817–2823.

Kou, P. M., Schwartz, Z., Boyan, B. D., & Babensee, J. E. (2011). Dendritic cell responses to surface properties of clinical titanium surfaces. *Acta Biomaterialia*, *7*(3), 1354–1363.

Kreiter, S., Diken, M., Selmi, A., Türeci, Ö., & Sahin, U. (2011). Tumor vaccination using messenger RNA: prospects of a future therapy. *Current Opinion in Immunology*, *23*(3), 399-

406

Leifer, C. A. (2017). Dendritic cells in host response to biologic scaffolds. In *Seminars in Immunology*. Academic Press.

Li, W. A., Lu, B. Y., Gu, L., Choi, Y., Kim, J., & Mooney, D. J. (2016). The effect of surface modification of mesoporous silica micro-rod scaffold on immune cell activation and infiltration. *Biomaterials*, *83*, 249–256.

Lu, L., Bonham, C. A., Chambers, F. G., Watkins, S. C., Hoffman, R. A., Simmons, R. L., & Thomson, A. W. (1996). Induction of nitric oxide synthase in mouse dendritic cells by IFN-gamma, endotoxin, and interaction with allogeneic T cells: nitric oxide production is associated with dendritic cell apoptosis. *Journal of Immunology*, *157*(8), 3577–3586.

Madden, L. R., Mortisen, D. J., Sussman, E. M., Dupras, S. K., Fugate, J. A., Cuy, J. L., … Ratner, B. D. (2010). Proangiogenic scaffolds as functional templates for cardiac tissue engineering. *Proceedings of the National Academy of Sciences of the United States of America*, *107*(34), 15211–15216.

Marshall, A., Irvin, C., Barker, T., Sage, K., Hauch, E., & Ratner, B. (2004). Biomaterials with tightly controlled pore size that promote vascular in-growth. In *ACS Polymer Preprints* (Vol. 45, pp. 100–101).

Marshall, A. J., & Ratner, B. D. (2005). Quantitative characterization of sphere-templated porous biomaterials. *AIChE Journal*, *51*(4), 1221-1232.

Matsiko, A., Gleeson, J. P., & O'Brien, F. J. (2015). Scaffold mean pore size influences mesenchymal stem cell chondrogenic differentiation and matrix deposition. *Tissue*

Engineering. Part A, *21*(3–4), 486–497.

Matzelle, M. M., & Babensee, J. E. (2004). Humoral immune responses to model antigen co-delivered with biomaterials used in tissue engineering. *Biomaterials*, *25*(2), 295–304.

Moffatt, S., & Cristiano, R. J. (2006). Uptake characteristics of NGR-coupled stealth PEI/pDNA nanoparticles loaded with PLGA-PEG-PLGA tri-block copolymer for targeted delivery to human monocyte-derived dendritic cells. *International Journal of Pharmaceutics*, *321*(1–2), 143–154.

Mograo, J., Da Costa, C. A., Gaspar, R., & Florindo, H. F. (2016). Modulation of dendritic cells by nanotechnology-based immunotherapeutic strategies. *Journal of Biomedical Nanotechnology*, *12*(3), 405–434.

Moser, M., & Murphy, K. M. (2000). Dendritic cell regulation of TH1-TH2 development. *Nature Immunology*, *1*(3), 199–205.

O'Rorke, S., Keeney, M., Pandit, A., O'Rorke, S., Keeney, M., Pandit, A., … Pandit, A. (2010). Non-viral polyplexes: scaffold mediated delivery for gene therapy. *Progress in Polymer Science*, *35*(4), 441–458.

Oliveira, M. I., Santos, S. G., Oliveira, M. J., Torres, A. L., & Barbosa, M. A. (2012). Chitosan drives anti-inflammatory macrophage polarisation and pro-inflammatory dendritic cell stimulation. *European Cells and Materials*, *24*(136), 152–153.

Palucka, K., & Banchereau, J. (2012). Cancer immunotherapy via dendritic cells. *Nature Reviews Cancer*, *12*(4), 265–277.

Park, J., & Babensee, J. E. (2012). Differential functional effects of biomaterials on dendritic cell

maturation. *Acta Biomaterialia*, *8*(10), 3606–3617.

Park, J., Wu, C. T., & Bryers, J. D. (2013). Chemokine programming dendritic cell antigen response: part I - select chemokine programming of antigen uptake even after maturation. *Immunology*, *139*(1), 72–87.

Perri, S., Driver, D. A., Gardner, J. P., Sherrill, S., Belli, B. A., Dubensky, T. W., & Polo, J. M. (2000). Replicon vectors derived from Sindbis virus and Semliki forest virus that establish persistent replication in host cells. *Journal of Virology*, *74*(20), 9802–9807.

Persano, S., Guevara, M. L., Li, Z., Mai, J., Ferrari, M., Pompa, P. P., & Shen, H. (2017). Lipopolyplex potentiates anti-tumor immunity of mRNA-based vaccination. *Biomaterials*, *125*, 81–89.

Phua, K. K. L., Leong, K. W., & Nair, S. K. (2013). Transfection efficiency and transgene expression kinetics of mRNA delivered in naked and nanoparticle format. *Journal of Controlled Release*, *166*(3), 227–233.

Platt, C. D., Ma, J. K., Chalouni, C., Ebersold, M., Bou-Reslan, H., Carano, R. A. D., … Delamarre, L. (2010). Mature dendritic cells use endocytic receptors to capture and present antigens. *Proceedings of the National Academy of Sciences*, *107*(9), 4287–4292.

Reddy, S. T., Swartz, M. A., & Hubbell, J. A. (2006). Targeting dendritic cells with biomaterials: developing the next generation of vaccines. *Trends in Immunology*, *27*(12), 573–579.

Rejman, J., Tavernier, G., Bavarsad, N., Demeester, J., & De Smedt, S. C. (2010). mRNA transfection of cervical carcinoma and mesenchymal stem cells mediated by cationic carriers. *Journal of Controlled Release*, *147*(3), 385–391.

Rice, W. L., Kaplan, D. L., & Georgakoudi, I. (2010). Two-photon microscopy for non-invasive, quantitative monitoring of stem cell differentiation. *PLoS ONE*, *5*(4), e10075.

Rodríguez-Gascón, A., del Pozo-Rodríguez, A., & Solinís, M. Á. (2014). Development of nucleic acid vaccines: Use of self-amplifying RNA in lipid nanoparticles. *International Journal of Nanomedicine*, *9*(1), 1833–1843.

Rutella, S., Danese, S., & Leone, G. (2006). Tolerogenic dendritic cells: cytokine modulation comes of age. *Blood*, *108*(5), 1435–1440.

Sallusto, F., Schaerli, P., Loetscher, P., Schaniel, C., Lenig, D., Mackay, C. R., … Lanzavecchia, A. (1998). Rapid and coordinated switch in chemokine receptor expression during dendritic cell maturation. *European Journal of Immunology*, *28*(9), 2760–2769.

Sandham, J. D., Hull, R. D., Brant, R. F., Knox, L., Pineo, G. F., Doig, C. J., … Kirby, A. (2010). Sipuleucel-T immunotherapy for castration-resistant prostate cancer. *New England Journal of Medicine*, *363*(5), 411–422.

Schlesinger, S. (2001). Alphavirus vectors: development and potential therapeutic applications. *Expert Opinion on Biological Therapy*, *1*(2), 177–191.

Shea, L. D., Smiley, E., Bonadio, J., & Mooney, D. J. (1999). DNA delivery from polymer matrices for tissue engineering. *Nature Biotechnology*, *17*(6), 551–554.

Shokouhi, B., Coban, C., Hasirci, V., Aydin, E., Dhanasingh, A., Shi, N., … Sechi, A. S. (2010). The role of multiple toll-like receptor signalling cascades on interactions between biomedical polymers and dendritic cells. *Biomaterials*, *31*(22), 5759–5771.

Son, C.-H., Bae, J.-H., Shin, D. Y., Lee, H.-R., Choi, Y. H., Yang, K., & Park, Y.-S. (2013).

Enhanced maturation and function of dendritic cells using hydrogel coated plate and antigen electroporation. *Immunological Investigations*, *42*(4), 1–15.

Stachowiak, A. N., & Irvine, D. J. (2008). Inverse opal hydrogel- collagen composite scaffolds as a supportive microenvironment for immune cell migration. *Journal of Biomedical Materials Research Part A*, *85*(3), 815–828.

Su, X., Fricke, J., Kavanagh, D. G., & Irvine, D. J. (2011). *In vitro* and *in vivo* mRNA delivery using lipid-enveloped pH-responsive polymer nanoparticles. *Molecular Pharmaceutics*, *8*(3), 774–787.

Uchida, S., Itaka, K., Chen, Q., Osada, K., Ishii, T., Shibata, M.-A., … Kataoka, K. (2012). PEGylated polyplex with optimized PEG shielding enhances gene introduction in lungs by minimizing inflammatory responses. *Molecular Therapy : The Journal of the American Society of Gene Therapy*, *20*(6), 1196–1203.

Ulmer, J. B., Donnelly, J. J., Parker, S. E., Rhodes, G. H., Felgner, P. L., Dwarki, V. J., … Friedman, A. (1993). Heterologous protection against influenza by injection of DNA encoding a viral protein. *Science*, *259*(5102), 1745–1749.

Underwood, R. A., Usui, M. L., Zhao, G., Hauch, K. D., Takeno, M. M., Ratner, B. D., … Fleckman, P. (2011). Quantifying the effect of pore size and surface treatment on epidermal incorporation into percutaneously implanted sphere-templated porous biomaterials in mice. *Journal of Biomedical Materials Research - Part A*, *98 A*(4), 499–508.

Wolff, J. A., Malone, R. W., Williams, P., Chong, W., Acsadi, G., Jani, A., & Felgner, P. L. (1990). Direct gene transfer into mouse muscle *in vivo*. *Science*, *247*(4949), 1465–1468.

Xie, Y., Yang, S. T., & Kniss, D. A. (2001). Three-dimensional cell-scaffold constructs promote efficient gene transfection: implications for cell-based gene therapy. *Tissue Engineering*, *7*(5), 585–598.

Yadava, P., Gibbs, M., Castro, C., & Hughes, J. A. (2008). Effect of lyophilization and freeze-thawing on the stability of siRNA-liposome complexes. *AAPS PharmSciTech*, *9*(2), 335–41.

Yamamoto, A., Kormann, M., Rosenecker, J., & Rudolph, C. (2008). Current prospects for mRNA gene delivery. *European Journal of Pharmaceutics and Biopharmaceutics*, *71*, 484–489.

Zanoni, I., Ostuni, R., Capuano, G., Collini, M., Caccia, M., Ronchi, A. E., … Granucci, F. (2009). CD14 regulates the dendritic cell life cycle after LPS exposure through NFAT activation. *Nature*, *460*(7252), 264–268.

Zhang, X.-Y., Liu, X.-G., Wang, W., Wang, W.-C., & Gao, X.-M. (2003). Anti-T-cell humoral and cellular responses in healthy BALB/c mice following immunization with ovalbumin or ovalbumin-specific T cells. *Immunology*, *108*(4), 465–473.

Zhang, X., Li, Y., Chen, Y. E., Chen, J., & Ma, P. X. (2016). Cell-free 3D scaffold with two-stage delivery of miRNA-26a to regenerate critical-sized bone defects. *Nature Communications*, *7*, 10376.